

1987

Improved ionization sources and detection methods for analytical mass spectrometry

Le Qun Huang
Iowa State University

Follow this and additional works at: <https://lib.dr.iastate.edu/rtd>

 Part of the [Analytical Chemistry Commons](#)

Recommended Citation

Huang, Le Qun, "Improved ionization sources and detection methods for analytical mass spectrometry" (1987). *Retrospective Theses and Dissertations*. 9751.
<https://lib.dr.iastate.edu/rtd/9751>

This Dissertation is brought to you for free and open access by the Iowa State University Capstones, Theses and Dissertations at Iowa State University Digital Repository. It has been accepted for inclusion in Retrospective Theses and Dissertations by an authorized administrator of Iowa State University Digital Repository. For more information, please contact digirep@iastate.edu.

INFORMATION TO USERS

The most advanced technology has been used to photograph and reproduce this manuscript from the microfilm master. UMI films the original text directly from the copy submitted. Thus, some dissertation copies are in typewriter face, while others may be from a computer printer.

In the unlikely event that the author did not send UMI a complete manuscript and there are missing pages, these will be noted. Also, if unauthorized copyrighted material had to be removed, a note will indicate the deletion.

Oversize materials (e.g., maps, drawings, charts) are reproduced by sectioning the original, beginning at the upper left-hand corner and continuing from left to right in equal sections with small overlaps. Each oversize page is available as one exposure on a standard 35 mm slide or as a 17" × 23" black and white photographic print for an additional charge.

Photographs included in the original manuscript have been reproduced xerographically in this copy. 35 mm slides or 6" × 9" black and white photographic prints are available for any photographs or illustrations appearing in this copy for an additional charge. Contact UMI directly to order.



300 North Zeeb Road, Ann Arbor, MI 48106-1346 USA



Order Number 8825472

**Improved ionization sources and detection methods for
analytical mass spectrometry**

Huang, Le Qun, Ph.D.

Iowa State University, 1987

U·M·I
300 N. Zeeb Rd.
Ann Arbor, MI 48106



**Improved ionization sources
and
detection methods
for analytical mass spectrometry**

by

Le Qun Huang

**A Dissertation Submitted to the
Graduate Faculty in Partial Fulfillment of the
Requirements for the Degree of
DOCTOR OF PHILOSOPHY**

Department: Chemistry

Major: Analytical Chemistry

Approved:

Signature was redacted for privacy.

In Charge of Major Work

Signature was redacted for privacy.

For the Major Department

Signature was redacted for privacy.

For the Graduate College

**Iowa State University
Ames, Iowa**

1987

Concepts and material in this dissertation entitled "Ion association by TOF-MS" and "summary and future research" are the partial basis of a patent (Ames Laboratory Record of Invention #BJG-165) being sought by the Iowa State University Research Foundation (ISURF #995) under the legal jurisdiction and contractual rights granted by the Department of Energy (DOE #S-65,049).

No preprints or descriptions of these sections can be given prior to reception of patent clearance which can be confirmed by the Iowa State University Research Foundation, Dan Griffen, Executive Director.

Patent clearance is expected to be received sometime during 1988.

TABLE OF CONTENTS

PREFACE	1
SECTION I. LASER DESORPTION TIME-OF-FLIGHT MASS SPECTROMETRY	
USING A 300 PICOSECOND UV LASER	5
INTRODUCTION	7
EXPERIMENTAL	9
Ion Source	9
Mass Analyzer	13
Detector and Data Acquisition System	13
Sample Preparation	14
Recording Data	15
RESULTS AND DISCUSSION	16
Laser Spot Size and Power	16
Mass Calibration	16
Mass Resolution	20
Laser Desorption Spectra	27
CONCLUSION	33
LITERATURE CITED	34
SECTION II. ION ASSOCIATION BY TIME-OF-FLIGHT MASS	
SPECTROMETRY	37
INTRODUCTION	39

EXPERIMENTAL	41
Data Acquisition	41
Sample Preparation	43
DATA TREATMENT	44
Multiplicity Measurement	44
Ion Association Measurement	44
RESULTS AND DISCUSSION	48
General Observation of Summed TOF Spectra	48
General Observation of Individual TOF Spectra	50
Study of Multiplicity	52
Study of Ion Association	56
SUMMARY AND CONCLUSION	64
LITERATURE CITED	65
 SECTION III. REDUCTION OF SIGNAL REFLECTION FOR RECORDING	
FAST PULSES FROM A MICROCHANNEL PLATE DETECTOR ..	67
INTRODUCTION	69
EXPERIMENTAL	70
RESULTS AND DISCUSSION	75
SUMMARY AND CONCLUSION	82
LITERATURE CITED	83
 SECTION IV. DIRECT DETERMINATION OF TRACE ELEMENTS IN	
SOLIDS BY LASER MASS SPECTROMETRY	84
INTRODUCTION	86
EXPERIMENTAL	87

Procedure	89
RESULTS AND DISCUSSION	92
Effects of Laser Power Density	92
Analytical Results for Steels and Brasses	94
Determination of Oxygen in Silicon	98
CONCLUSION	101
LITERATURE CITED	102
SECTION V. SCINTILLATION-TYPE ION DETECTION FOR INDUCTIVELY COUPLED PLASMA MASS SPECTROMETRY	104
INTRODUCTION	106
EXPERIMENTAL	109
ICP-MS Apparatus	109
Scintillation Detector	111
Data Acquisition	112
Solutions and Standards	113
RESULTS AND DISCUSSION	114
General Observations	114
Precision of Isotope Ratio Measurements	115
Detector "Fatigue"	117
Linear Dynamic Range and Stability	120
Detection Limits and Sensitivities	122
CONCLUSION	125
LITERATURE CITED	126
SUMMARY AND FUTURE RESEARCH	128

APPENDIX A	132
APPENDIX B	133
ACKNOWLEDGEMENTS	134

PREFACE

From its inception, mass spectrometry (MS) has dealt with ionic species in the gas phase and with the exploitation of the knowledge thus gained to carry out direct characterization and quantitation in solids and solutions -- media closely resembling the natural environment of these molecules. This remarkable transition is possible with the explosive growth in analytical utility of condensed-phase ionization methods. Some new so-called "soft ionization" techniques, including laser desorption (LD), ^{252}Cf plasma desorption (^{252}Cf -PD), secondary ion mass spectrometry (SIMS), fast atom bombardment (FAB), and field desorption (FD), transfer only a small amount of excitation energy to the specimen to desorb intact molecular ions with limited fragments, and these techniques have been growing into perhaps the most vital branch of the field today for high mass organic and biochemical analysis. Other ionization techniques such as inductively coupled plasma (ICP), glow discharge, and high power laser ionization, provide sufficient energy to atomize and ionize samples completely ("hard ionization"), and they have shown considerable promise of making the sensitivity, selectivity, and dynamic range of MS available for elemental analysis.

It is the overall purpose of this dissertation to describe the improvements in the "soft" and "hard" ionization sources as well as detection methods for analytical mass spectrometry. The format of this dissertation is divided into five sections. Each section stands alone as a complete manuscript with figures, tables and literature cited.

The first section describes a new time-of-flight mass spectrometer (TOF-MS) constructed in our group. A 300 ps pulsed N_2 laser ($\lambda = 337$ nm) was successfully used with the TOF-MS to study ion formation from various solid samples. Improved techniques were incorporated for fast ion detection and acquisition. For inorganic specimens the mass resolution was ~ 2000 at $m/z = 400$, a considerable improvement over earlier reports for instruments using a linear ion optical path. Cationized parent ions and structurally significant fragments were obtained from sucrose, in contrast to previous observations and predictions for sub-nanosecond UV laser desorption. Some laser desorption spectra are shown to demonstrate the operation and analytical capability of the system.

This TOF-MS is designed specifically to allow the investigation of the information available from individual TOF spectra. This capability permits investigation of ion association of different ions due to their co-desorption, chemical association, or formation from common precursors. Some specific steps were taken to permit such studies. First, the aforementioned short duration ion source (300 ps, 10 μ J laser desorption) produces only a few ions per TOF spectrum. We therefore could observe ion associations from individual mass spectra which might otherwise be masked when the number of ions-per-pulse is very high as in most ion sources for TOF-MS. Second, a data acquisition system including special hardware and software has been developed to allow convenient recording of spectra from laser individual shots for subsequent study. Third, classical statistical methods were used to treat the data for the study of ion association.

In the second section of this dissertation this approach is described and the results of ion association studies are given for LD-TOF-MS spectra of CsI and a superconducting sample, $\text{YBa}_2\text{Cu}_3\text{O}_7$.

Improvement in the application of the microchannel plate detector (MCPD) to TOF-MS is shown in this dissertation in Section three. Ion signal transmission yielding low reflection characteristics is demonstrated for a MCPD equipped with a metal plate anode. Flexible movement of the detector within the vacuum chamber is achieved by coupling with a 50 Ω vacuum cable, appropriate shielding of the connections, and the use of a commercial 50 Ω impedance matched vacuum flange.

Two projects in "hard ionization" methods were also undertaken. The fourth section deals with high power laser mass spectrometry (LMS). The laser ionization is so "hard" that the assumption generally made is that the various elements are completely ionized in the laser miniplasma and detected by the mass spectrometer with uniform efficiency so that calibration standards that closely match the matrix composition of the sample are unnecessary. The uniformity of response for impurity elements in metals is tested by analyzing standard reference materials (SRMs). The results show generally good uniformity ($\pm 30\%$) for metal elements. They also indicate that LMS may ultimately achieve quantitative determination of trace elements in solids without standards when even "harder" ionization, i.e., a higher laser power density of $>10^{10} \text{ W cm}^{-1}$, is achieved.

The final project represents an improvement in ICP-MS, which is presented in Section five. A scintillation-type ion detector has been constructed and evaluated for ICP-MS. This detector has a linear range up to 2×10^6 counts s^{-1} , yields isotope ratios with precisions that are generally close to those expected from counting statistics, shows no gain fatigue after scanning across an intense peak, and yields signal stability of $\pm 5\%$ relative standard deviation during two hours. These performance figures are comparable to or better than those obtained previously with this particular instrument using a Channeltron electron multiplier as a detector. Detection limits and sensitivities obtained with the scintillation detector were similar to those obtained with a Channeltron. The scintillation detector also does not require rejuvenation or replacement as a Channeltron does.

**SECTION I. LASER DESORPTION TIME-OF-FLIGHT
MASS SPECTROMETRY USING A 300 PICOSECOND UV LASER**

LASER DESORPTION TIME-OF-FLIGHT MASS SPECTROMETRY
USING A 300 PICOSECOND UV LASER

L. Q. HUANG, R. J. CONZEMIUS, G. A. JUNK AND R. S. HOUK
AMES LABORATORY-USDOE AND DEPARTMENT OF CHEMISTRY
IOWA STATE UNIVERSITY

INTRODUCTION

The combination of lasers with mass spectrometry has grown rapidly in recent years (1-3), particularly in laser desorption mass spectrometry (LD-MS) for analysis of thermally labile or highly polar organic and biologically significant compounds (4-8). LD and other "soft-ionization" techniques such as fast atom bombardment (FAB) (9), secondary ion mass spectrometry (SIMS), (10), field desorption (FD) (11), and ^{252}Cf plasma desorption (12) have greatly enhanced the ability of MS to characterize complex substances.

TOF-MS is ideally suited to LD because both the analyzer and the source are pulsed techniques and TOF-MS has a theoretically unlimited mass range as well as efficient ion transmission. The renaissance of TOF-MS has also been stimulated by the rapid development of fast electronics and computer techniques and by the improvements in mass resolution of the TOF analyzer (13). Mamyrin and co-workers have introduced an ion reflector to enhance the resolving power (14). Poschenrieder has proposed the use of a sector field to achieve isochronous angular and energy focusing (15). Efforts have also been made to shorten the duration of the ion production, e.g., the use of a short pulse laser by Tsong and Kinkus in a TOF-MS atom-probe study (16). All lasers, nevertheless, currently used for LD-TOF-MS are pulsed in the range of 5 ns - 50 ns (7,8).

Earlier work suggested that sub-nanosecond, pulsed UV lasers might cause extensive fragmentation and thus would not be useful for LD of large organic molecules (17). This dissertation shows that intact

molecular ions and structurally significant fragments can be obtained from sucrose by LD with a fast laser. We also demonstrate reasonably high mass resolution and mass assignment accuracy for inorganic films which serve as substrates for organic specimens.

EXPERIMENTAL

The TOF-MS system was constructed locally and is depicted in Figure 1. Instrumental components and typical operating parameters are given in Table 1.

Ion Source

The ion source was designed with an angle ϕ of -90° between the laser beam and sample surface and an angle θ of 90° between the ion optical axis and the sample surface (see insert of Fig. 1). Characteristics of the pulsed N_2 laser are also given in Table 1. The laser was focused at the specimen surface prior to insertion of samples and the energy incident to the specimen was adjusted by limiting the maximum laser beam cross section with an iris located in front of the window on the vacuum chamber. The laser was initially aligned by carefully adjusting the beam into focus at the specimen surface by moving a quartz lens located inside of the vacuum chamber while watching the laser spot on burn paper. The desorbed ions were accelerated using a grounded coplanar grid of 90% transparency spaced 3 mm from the surface of the specimen. The ion source utilized an ion accelerating field which was constant in time as opposed to a system described previously (20). Formation of ions very close to the equipotential surface of the thin film which is perpendicular to the spectrometer axis should yield a relatively narrow axial ion velocity distribution and improved mass resolution (21).

Figure 1. Schematic diagram of the LD TOF-MS instrument

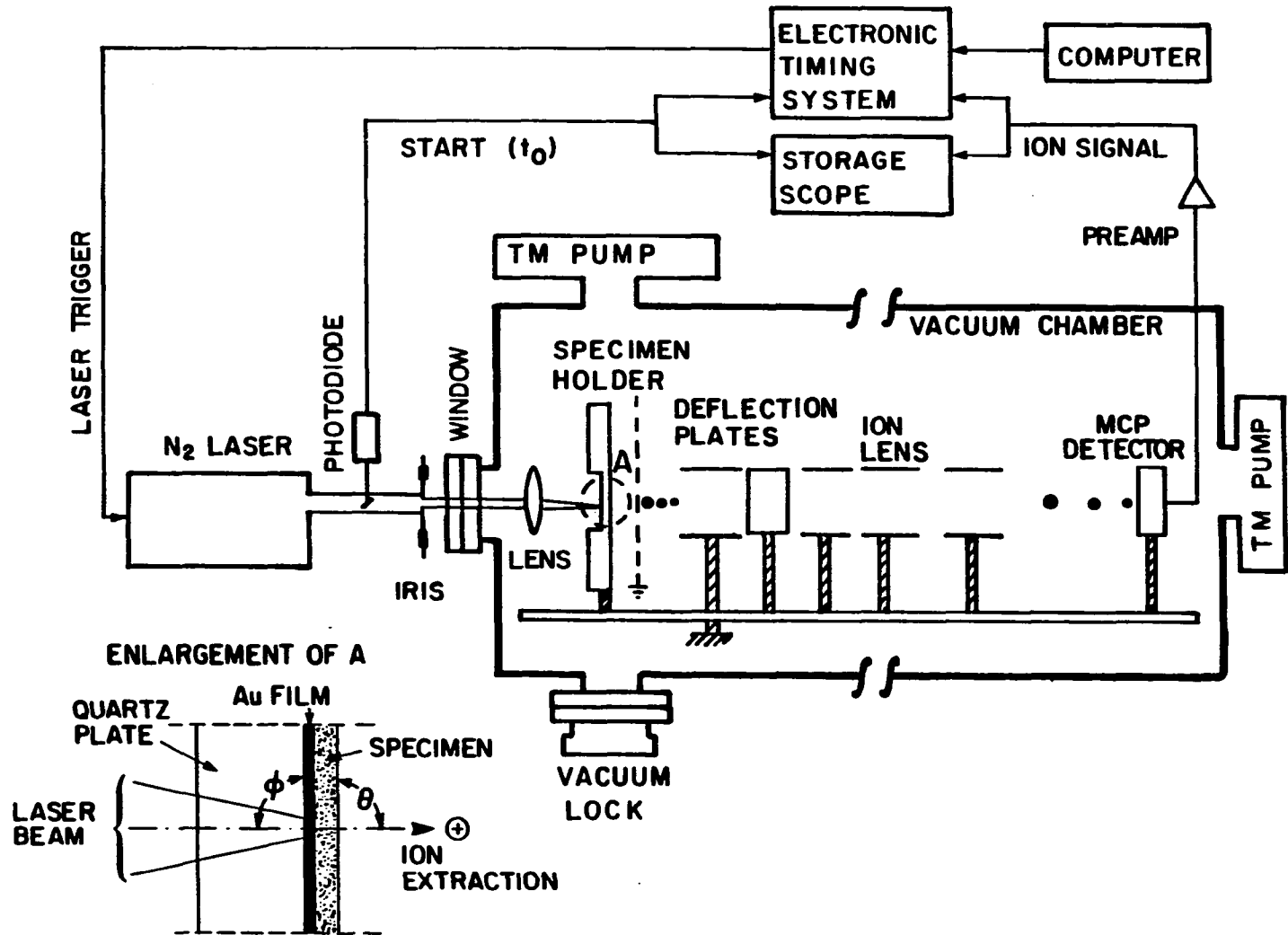


Table 1. Instrumental Facilities

Components	Operating conditions, materials, or dimensions	
N₂ Laser: Photochemical Research Associates Inc., model LN 120	Wavelength Pulse Width, nominal Repetition rate Energy/pulse Lens focus length	337.1 nm 300 ps 1-20 Hz 10-70 μ J 2.5 cm
Ion source: Ames Laboratory construction	Accelerating voltage Accelerating region Gold film thickness Quartz plate thickness	+ 5 kV 3 mm 50 nm 1.5 mm
TOF Mass Analyzer and Ion Optics: Ames Laboratory Construction	Flight path length Flight path diameter Operating pressure Deflection plate voltages Einzel lens voltage	1.2 m 15 cm 8×10^{-8} torr $\pm 0 \sim 100$ V ~ 1800 V
Vacuum Pumps: Turbomolecular pumps: Leybold-Heraeus Vacuum Product Inc., model TMP 150 and TMF 350	Pumping speeds	150 and 350 $l s^{-1}$
Ion Detector: Microchannel Plates: Varian, model VUW8946 Housing: Ames Laboratory Construction (18)	Voltage bias on the three stages	-1800V, -900V, -100V
Data Acquisition System: Time-to-digital convertor: LeCroy Research Systems Corporation, model 4208 Fast Storage Scope: Tektronix, Inc., model 7834 Computer: Hewlett Packard, model Vectra 45	Operating principles and conditions described in Ref. (19).	

A vacuum lock and direct insertion probe permitted changing of specimens without greatly disturbing the vacuum in the main system, i.e., after insertion of a new sample through the vacuum lock, the base operating pressure was obtained within 5 minutes. The sample holder of the probe was designed to contain a 1 cm² quartz plate upon which the specimen was deposited. The holder was made with a lock and key design to assure accurate resetting of the specimen position in the source chamber.

Mass Analyzer

The ion source, X-Y beam deflection plates, an Einzel lens, and an ion detector were constructed as modules and attached to precision ground rods. The rods served as an ion optical rail inside the chamber and permitted the vacuum chamber to be constructed without the high precision needed for positional accuracy over long distances. The rods and module placement also facilitated drastic changes in the ion optical scheme and provided mechanical alignment for the ion optical components and detector.

Detector and Data Acquisition System

A microchannel plate assembly with a fast electrical response and low reflection characteristics was constructed for ion detection (18).

A unique data acquisition system with 1 ns time resolution was

developed for the TOF system. The "start" signal (time zero) for an eight channel time-to-digital convertor (TDC) was provided by a photodiode which detected the laser pulse. Amplified pulses from the microchannel plate detector supplied the "stop" signals for the TDC. The threshold setting in the TDC for activating the stop signals was set at fifty percent of the nominal peak signal received for single ions. Thus, the TOF start-of-sweep was synchronized with the actual laser pulse and the TDC measured the time required for ions to reach the detector. The timing system was controlled with a computer, which also stored the measured arrival times and displayed the resulting spectra. For initial adjustment of the laser energy and data acquisition, the mass spectra from individual laser pulses could be viewed directly on a storage oscilloscope. A complete description of the data acquisition system will be given in reference 19.

Sample Preparation

A thin layer of Al or Au (~ 50 nm) was vacuum evaporated onto a quartz plate prior to sample deposition. The thin film facilitated uniform specimen deposition, minimized charge build up on the specimen, and served as a substrate for absorption of laser energy in the immediate environment of the specimen.

Samples of cesium iodide or sucrose were dissolved in deionized water at 10^{-2} M. Methanol was added to the sample solution at 10 to 50 percent to facilitate uniform deposition onto the gold film. The

sucrose solution was doped with a small amount of sodium chloride to promote cationization. The sample was deposited with a micropipet, typically using 1 μ L followed by air drying. The deposition was repeated 3-5 times until a thin layer of sample (~ 30 ng) was barely visible on the substrate.

Recording Data

Ion beam transmission was maximized by adjusting voltages on the deflection plates and on the Einzel lens. The threshold laser energy was found by setting the iris to the smallest diameter that still yielded detectable ion signals. Then the spectra were obtained using an accumulation of 30 to 1000 sweeps. Data acquisition was terminated when the ion signal decreased significantly due to damage of the sample by repeated laser shots.

RESULTS AND DISCUSSION

Laser Spot Size and Power

Erosions caused by focused laser excitation of an Au film are shown in Figure 2. These typical spot sizes were $60 \times 180 \mu\text{m}^2$ or $\sim 10^{-4} \text{ cm}^2$. Threshold energy levels for observing spectra were $\sim 10 \mu\text{J}$. Thus the typical laser power density at the substrate was about $3 \times 10^8 \text{ W cm}^{-2}$ and the energy density $\sim 0.15 \text{ J cm}^{-2}$.

Mass Calibration

The ion mass-to-charge ratio was calculated from the equation $(m/z)^{1/2} = a + bt$, where $t = \text{time}$ and the constants a and b were determined from two peaks corresponding to known masses. An illustration of the accuracy in mass assignment is given in Table 2 for the spectrum shown in Figure 3 of an Al film where the known masses were the Na^+ peak at m/z 22.990 and the Al_3^+ peak at m/z 80.945. These results show that an average mass accuracy of $\pm 0.017 \text{ u}$ was achieved for the indicated mass range. Accurate mass assignments were obtained even when less than 20 ions were measured, i.e., for AlH^+ , AlH_2^+ , Al_2H_3^+ , AlCa^+ and Al_2OH_4^+ through Al_3O_2^+ . These small Δm values represent excellent performance of the system. It is only fair to say that mass calibration and assignment are much more difficult for high mass, particularly for organic specimens.

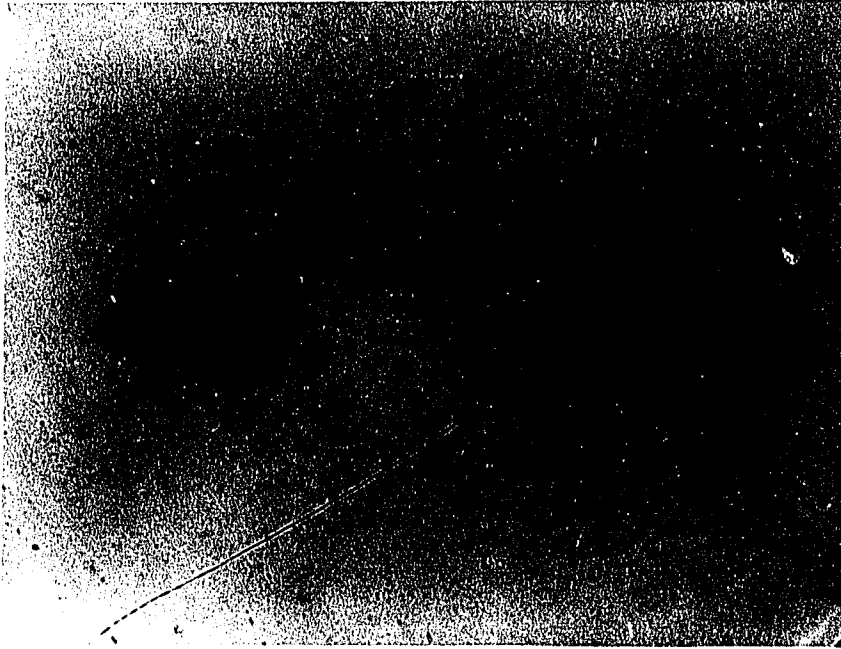


Figure 2. Photograph of two laser erosions taken by using 100 laser pulses at each of two sites. The specimen is ~ 50 nm thin gold film

Table 2. Mass calibration for TOF spectrum of an Al film

Time ^a (μ s)	m/z (Expl ^b) (u)	m/z (Real) (u)	Δ Mass (u)	Possible ion
7.120	22.990	22.990	-	Na ⁺
7.711	26.969	26.982	-0.013	Al ⁺
7.856	27.992	27.989	-0.007	AlH ⁺
8.000	29.035	28.997	0.038	AlH ⁺
9.268	38.979	38.964	0.015	³⁹ K ⁺
9.504	40.989	40.962	0.027	⁴¹ K ⁺
10.904	53.971	53.963	0.008	Al ₂ ⁺
11.002	54.954	54.971	-0.017	Al ₂ H ⁺
11.103	55.966	55.979	-0.013	Al ₂ H ₂ ⁺
11.204	56.986	56.987	-0.001	Al ₂ H ₃ ⁺
12.414	69.974	69.958	0.016	Al ₂ O ⁺
12.501	70.964	70.966	-0.002	Al ₂ OH ⁺
12.589	71.968	71.974	-0.006	Al ₂ OH ₂ ⁺
12.676	72.966	72.981	-0.015	Al ₂ OH ₃ ⁺
12.762	73.960	73.989	-0.029	Al ₂ OH ₄ ⁺
13.351	80.945	80.945	-	Al ₃ ⁺
13.436	81.980	81.954	0.028	Al ₃ H ⁺
13.516	82.971	82.960	0.010	Al ₃ H ₂ ⁺
14.611	96.962	96.940	0.022	Al ₃ O ⁺
14.684	97.932	97.947	-0.015	Al ₃ OH ⁺
15.770	112.976	112.934	0.042	Al ₃ O ₂ ⁺

^aMeasured times represent the centroids of the peaks.

^b $(m/z)^{1/2} = bT + a$ where $b = 0.6745$, $a = -0.0074$ from Na⁺ and Al⁺.

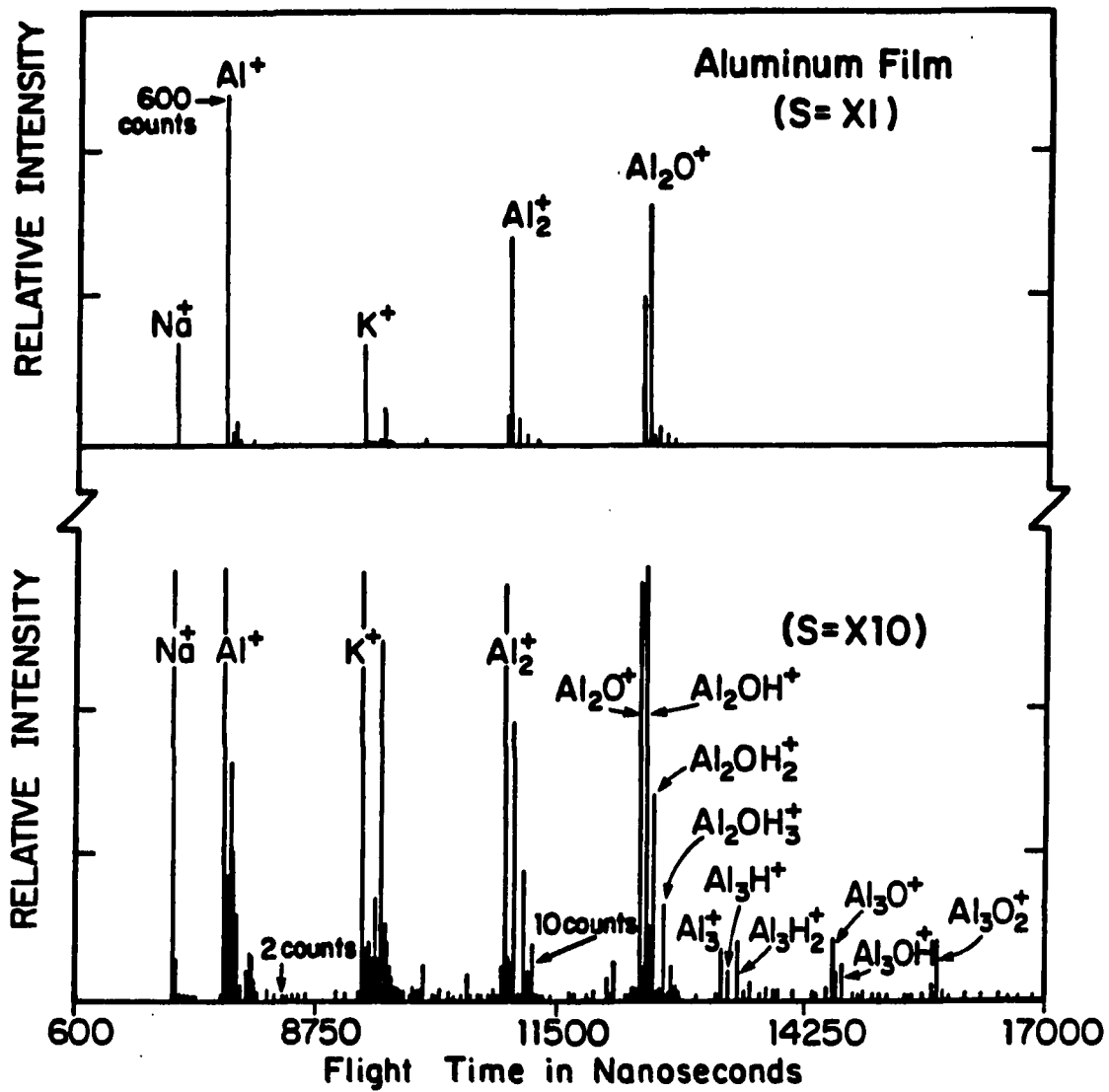


Figure 3. Laser desorption TOF spectrum of an Al film (~ 50 nm) on a quartz substrate averaged over 1000 laser shots

Mass Resolution

The TOF spectrum of a thin gold film is shown in Figure 4. The Au_2^+ (m/z 394 in Figure 4b) is 6 ns full width at half maximum (FWHM). With a total flight time of 23,833 ns, the corresponding mass resolution is ~ 2000 using the common equation of R (50% valley) = $(1/2) (t/\Delta t)$ (22). An alternate definition of the mass resolution is to measure peak width at 10% valley. With this criterion R = total flight time / Δt and Figure 4b indicates a Δt of 11 ns which yields a mass resolution of ~ 2200 .

The mass resolution obtained here is higher than reported with other linear instruments for LD-TOF-MS (13) and better than or comparable to that obtained with the energy-focused TOF of much more elaborate designs, e.g., typical mass resolutions of 800 achieved with a commercial TOF-MS equipped a reflector (4). Although the resolution value was achieved here with a carefully prepared thin gold film, similar results have also been obtained with CsI specimens as shown in Figure 5.

The various contributions to peak broadening for TOF-MS with linear ion optics have been described (23,24) and an assessment of the individual contributions is pertinent. The time spread induced by the laser pulse width (300 ps) is negligible compared to the observed ion pulse width (~ 10 ns). The detector rise time of 1.5 ns (18) and the electronic jitter of less than 3 ns (19) make only minor contributions. Space charge effects should be very small due to the low number of ions (10 - 100) produced per laser shot (25). Peak broadening due to

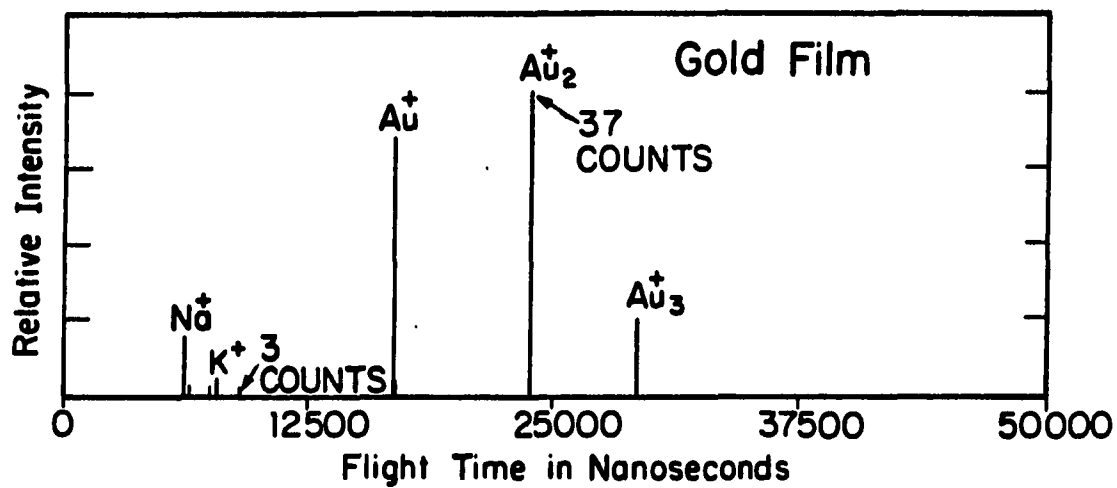


Figure 4a. Laser desorption TOF spectrum of an Au film on a quartz substrate averaged over 50 laser shots

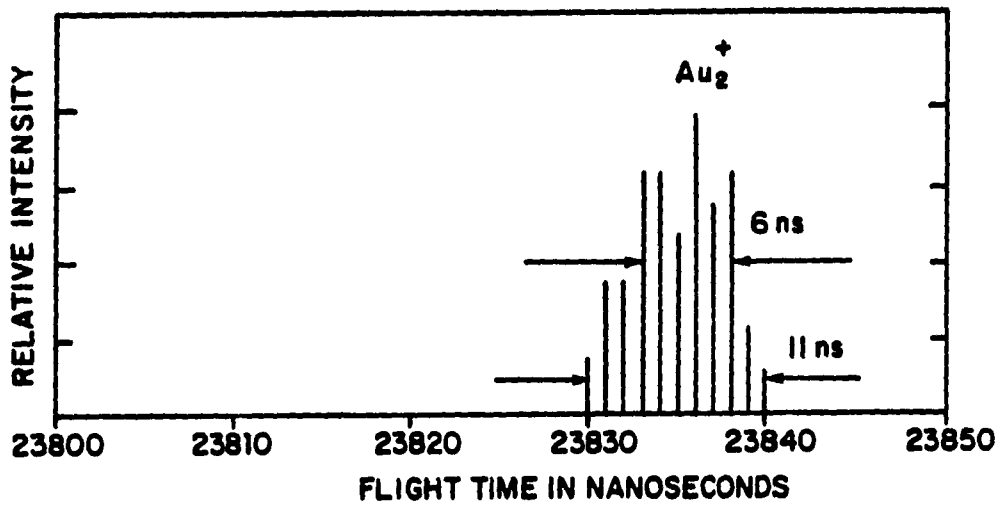


Figure 4b. Laser desorption TOF spectrum of an Au film on a quartz substrate averaged over 500 laser shots with 1 ns time slice recording showing Au_2^+ peak width of 6 ns (FWHM) and 11 ns (10% valley)

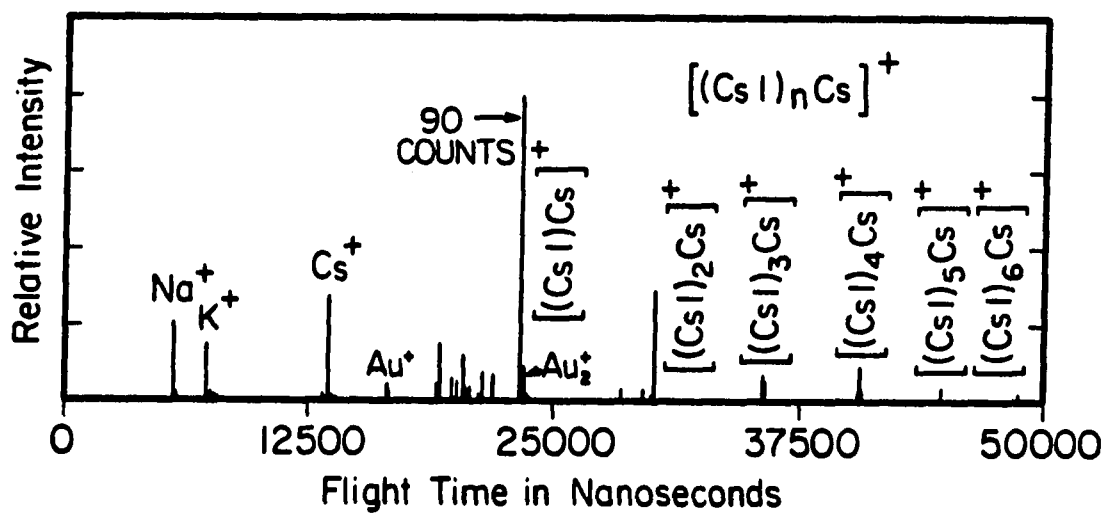


Figure 5a. Laser desorption TOF spectrum of a CsI specimen on a quartz substrate averaged over 100 laser shots

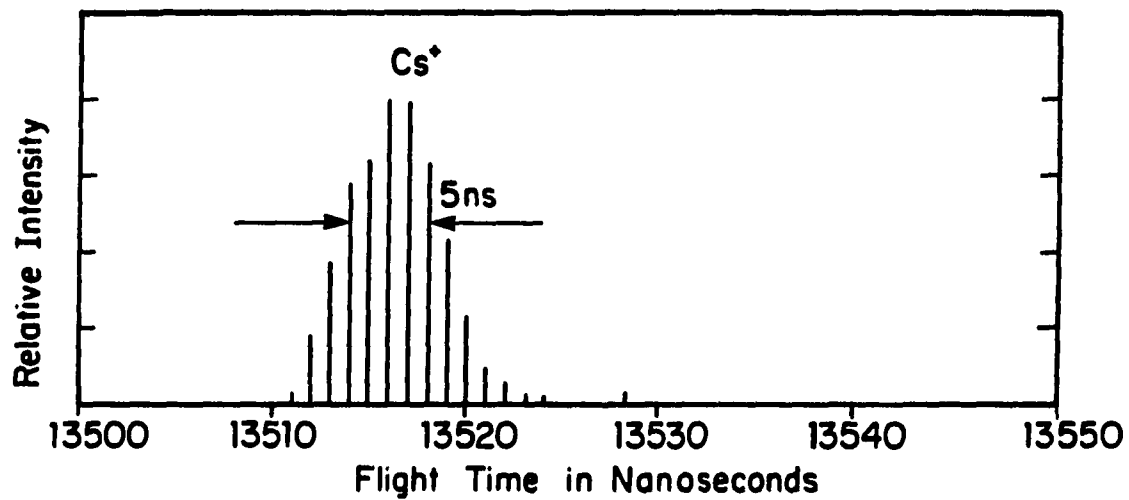


Figure 5b. Laser desorption TOF spectrum of a CsI specimen on a quartz substrate averaged over 1000 laser shots with 1 ns time slice recording showing Cs^+ peak width of 5 ns (FWHM)

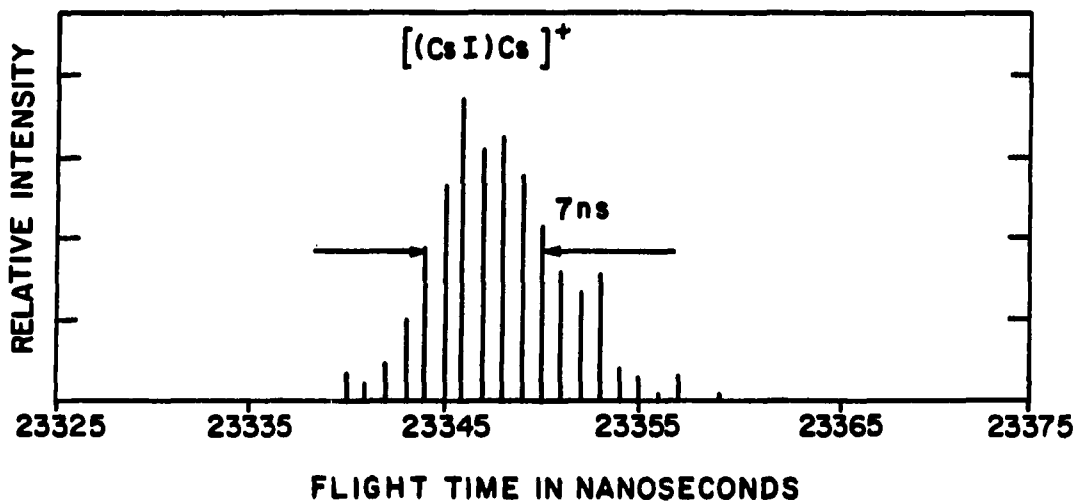


Figure 5c. Laser desorption TOF spectrum of a CsI specimen on a quartz plate substrate averaged over 1000 laser shots with 1 ns time slice recording showing $[(CsI)Cs]^+$ peak width of 7 ns (FWHM)

misalignment should not be a major factor because the rod and module design provide excellent mechanical alignment. The production of ions in LD along the flat plane of the substrate minimizes the deleterious effects of spatial distributions of ion production observed in ionization of gaseous samples (24).

For linear TOF-MS ion optics without kinetic energy compensation devices (14, 15) the ion kinetic energy spread is frequently the main cause of peak broadening (24). Others (26) have found kinetic energy spreads of ~ 1 eV for LD using power densities of $\sim 10^7$ W cm⁻². For our TOF-MS a peak width of 6 ns (FWHM) at $m/z = 400$ corresponds to an energy spread of 2.5 eV which seems reasonable.

Delayed emission of ions due to latent thermal desorption following the laser pulse (27) requires specially pulsed ion accelerating fields to compensate for the time spread (20). In the present work, the goal is to absorb the laser energy in a thin film at very low energy densities and in very short time periods. This should provide the rapid thermal transient necessary for ion desorption of intact molecules but inhibit the delayed emission since the energy absorbed is small. A spectrum of an Al film (Figure 3) was obtained at a higher energy density (0.7 J cm⁻²). Some small peak tailing was observed for Na⁺, Al⁺, K⁺, and Al₂O⁺. For the Au film the energy density was lower (~ 0.1 J cm⁻²) and much less peak tailing was observed. Gold is chemically stable, is easily vapor deposited, and should be a good candidate for an absorbing substrate especially if the peak shape of a sample desorbed with the gold retains the same peak profile. The CsI spectrum (CsI deposited on an Au film) showed narrow peak widths similar to the Au

spectrum although some minor delayed ion emission is indicated by the small tail on the high mass side of Na^+ and K^+ , barely visible in Figure 5a. The minor broadening of 2 to 3 ns on the high mass side for $[(\text{CsI})\text{Cs}]^+$ shown in Figure 5c compared to Cs^+ in Figure 5b could be caused by delayed ion emission and/or metastable decomposition. These spectra also indicate that the time resolution of the detection system is sufficient to follow slight changes in peak shape.

Generally, the resolving power for organic molecules in LD-TOF-MS is poorer than for inorganic species, probably due to extensive metastable decay along the flight path (13, 23) as well as to delayed emission of organic ions from the ion source. Evidence for this lower resolution for organic molecules was also observed here as indicated in the spectrum of sucrose shown in Figure 6. Delayed emission is not immediately evident but could be masked by the broad peaks. Thus the achievable mass resolution for organic specimens is not yet determined but is expected to be high if ion desorption can be accomplished with low laser energy density through improved preparation of specimens and if an ion reflector is used to reduce the broad metastable components of the peaks (14).

Laser Desorption Spectra

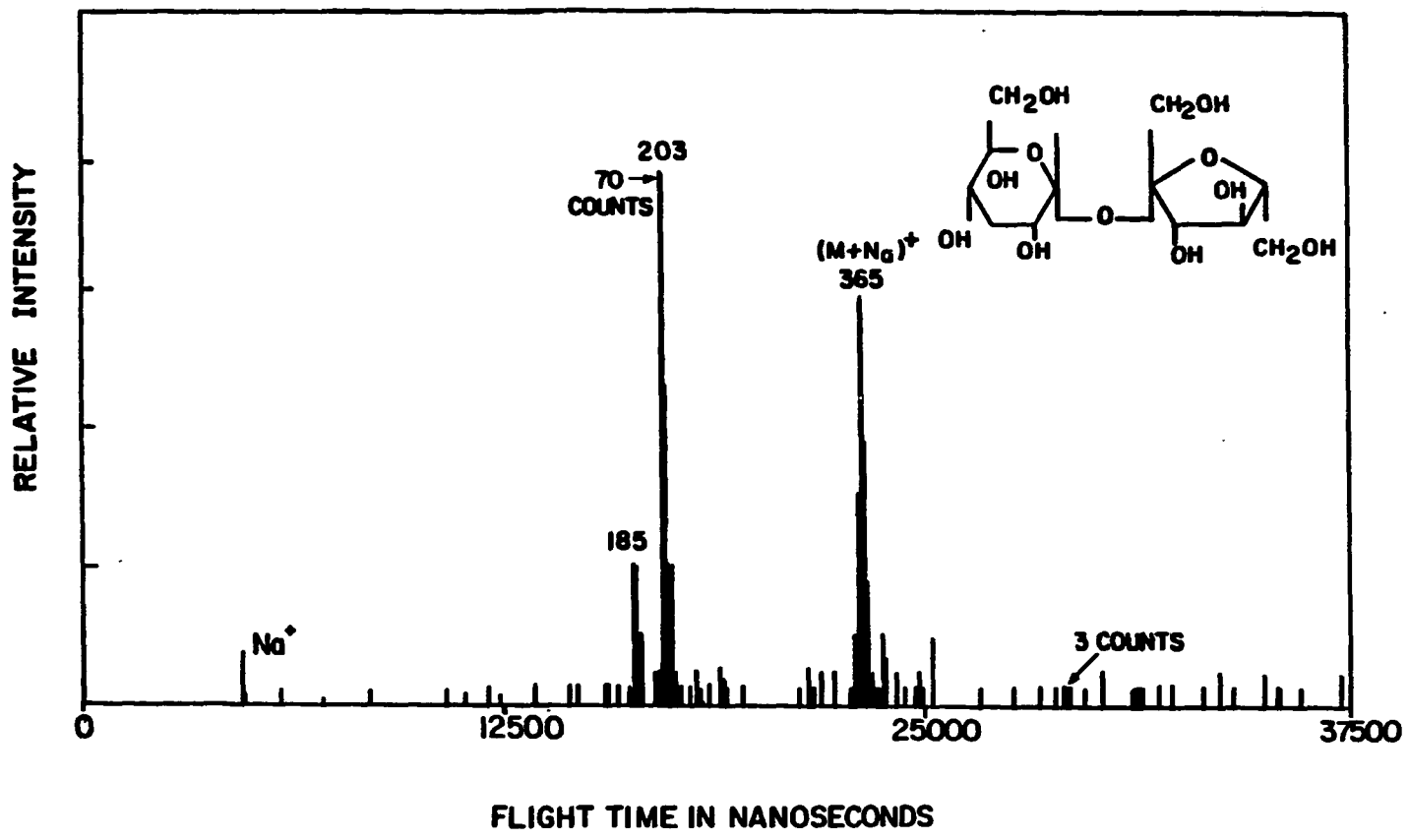
No other spectra of Al films produced by LD ionization were found in the literature. The Al film was exposed to air for several days before insertion into the ion source and thus aluminum oxide and hydroxide peaks, indicative of an active metal substrate, were observed as shown

in Figure 3. The backgrounds observed in the spectra were always three counts or less and were usually zero. The low background level is probably due to the method used for setting the threshold for stop signals in the TDC and also to the relatively small number of total ions utilized for determining the mass spectra.

The spectrum for the Au film is much simpler than for the Al film and the polymeric ions of gold are very useful for mass calibration. In the spectrum for CsI, the Au ion signals are greatly attenuated. The cluster ions, $[(\text{CsI})_n\text{Cs}]^+$, up to $n = 6$ at an m/z of 1691.7, are observed in agreement with earlier studies (28,29). However, the larger cluster ions ($n > 6$) reported by others were not observed in the present work due to the limited number of total ions in the spectrum.

Sucrose is a good test case for LD studies of organic compounds because its spectral characteristics have been studied extensively (30,31) and it represents a class of compounds that exhibit strong thermal degradation upon vaporization (32). The three major peaks from sucrose are evident in Figure 6 and were identified as $[\text{M}+\text{Na}]^+$ at $m/z = 365$ and cationized fragments at $m/z = 203$ and 185. The spectrum in Figure 6 is quite similar to that observed by McCreery and Gross with Fourier transform mass analysis (30) but shows much less fragmentation than that reported by Heinen (31) using a commercial LD-TOF-MS. Both of these studies were performed using lasers having longer pulse widths (5 - 10 ns) than that used in the present work. The detection of intact parent ions and structurally significant fragments from LD with our sub-nanosecond UV laser differs considerably from the report of Karas et al. (17) who observed extensive decomposition with a 30 ps laser at 265

**Figure 6. Laser desorption TOF spectrum of sucrose
averaged over 100 laser shots**



nm even at threshold laser power levels. This type of decomposition was not observed in the present work even at laser power levels seven times higher than the threshold value used to obtain the spectrum given in Figure 6.

A spectrum obtained from a Ni mesh is shown in Figure 7. The isotope ratio $^{58}\text{Ni}/^{60}\text{Ni}$ as calculated by integrating the total counts of the peaks is 2.5, which is in reasonable agreement with the natural abundance of 2.2.

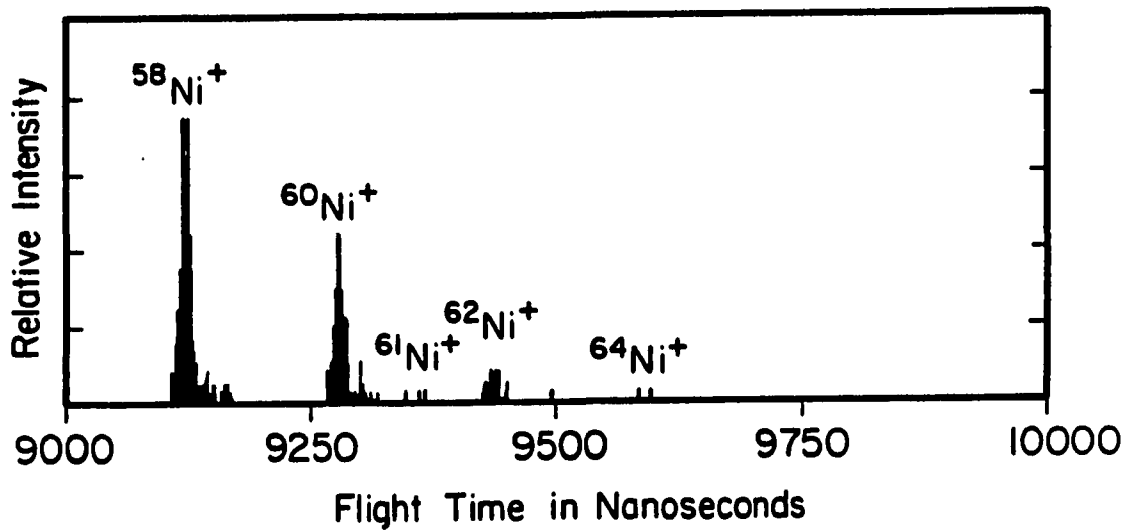


Figure 7. Laser desorption TOF spectrum of a Ni mesh averaged over 1000 laser shots

CONCLUSION

It would be a significant advance if the mass resolution of 2000 obtained with inorganic specimens could be retained with nonvolatile and thermally labile organic specimens. This advance will require more detailed studies of substrate preparation, specimen deposition, faster lasers, and a variety of different samples.

LITERATURE CITED

1. Conzemius, R. J.; Capellen, J. M. Int. J. Mass Spectrom. Ion Phys. 1980, 34, 197.
2. Cotter, R. J. Anal. Chem. 1984, 56, 485A.
3. Conzemius, R. J.; Junk, G. U. S. Department of Energy Report 1986, DOE-MBM-7001005.
4. Hillenkamp, F. "Laser Induced Ion Formation from Organic Solids", Benninghoven A. Ed.; Springer-Verlag: Berlin, 1983; P. 190.
5. Vestal, M. L. Mass Spectrom. Rev. 1983, 2, 447.
6. Burlingame, A. L.; Baillie, T. A.; Derrick, P. J. Anal. Chem. 1986, 58, 165R.
7. Hillenkamp, F. H. "Laser Desorption Mass Spectrometry", Colton R. J. Ed.; Spinger-Verlag: Berlin, 1985; P. 471.
8. Karas, M.; Bahr, U. Trends. Anal. Chem. 1986, 5, 90.
9. Barber, M.; Bordoli, R. S.; Elliot, G. J.; Sedgwick, R. D.; Tyler, N. Anal. Chem. 1982, 54, 645A.
10. Benninghoven, A.; Sichtermann, W. Anal. Chem. 1978, 50, 1180.
11. Beckey, H. D. "Principles of Field Ionization and Field Desorption Mass Spectrometry"; Pergamon: Oxford, 1977.
12. MacFarlane, R. D.; Torgerson, D. F. Science 1976, 191, 920.
13. Price, D.; Milnes, G. Int. J. Mass Spectrom. Ion Processes 1984, 60, 61.
14. Mamyrin, B. A.; Karataev, V. I.; Shmikk, D. V.; Zagulin, V. A. Soviet Phys. 1973, 37, 45.
15. Poschenrieder, W. P. Int. J. Mass Spectrom. Ion Phys. 1972, 9, 357.

16. Tsong, T. T.; Kinkus, T. J. Phys. Rev. B. Cond. Matl. 1984, 29, 529.
17. Karas, M.; Bachmann, D.; Hillenkamp, F. Anal. Chem. 1985, 57, 2935.
18. Huang, L. Q.; Conzemius, R. J.; Holland, G. E.; Houk, R. S. Anal. Chem. submitted.
19. Conzemius, R. J.; Adduci, D; Huang, L. Q.; Junk, G. A.; and Houk, R. S. Department of Chemistry, Iowa State University; to be published.
20. Van Breemen, R. B.; Snow, M.; Cotter, R. J. Anal. Chem. 1983, 49, 35.
21. Standing, K. G.; Beavis, R.; Eng, W.; Schneler, B. Int. J. Mass Spectrom. Ion Phys. 1983, 53, 125.
22. Walter, K.; Boesl, U.; Schlag, E. W. Int. J. Mass Spectrom. Ion Processes 1986, 71, 309.
23. Della-Negra, S.; Le Beyec, Y. Anal. Chem. 1985, 57, 2035.
24. Opsal, R. B.; Owens, K. G.; Reilly, J. P. Anal. Chem. 1985, 57, 1884.
25. Cotter, R. J.; Honovich, J.; Olthoff, J. "Time-of-flight Instrumentation for Laser Desorption, Plasma Desorption and Liquid SIMS", Colton, R. J. Ed.; Springer-Verlag: Berlin, 1985; P. 182.
26. Van Der Peyl, G. J. O.; Van Der Zande, W. J.; Kistemaker, P. G. Int. J. Mass Spectrom. Ion Processes 1984, 62, 51.
27. Cotter, R. J. Trends Anal. Chem. 1982, 1, 307.
28. Campana, J. E.; Barlak, T. M.; Colton, R. J.; Decorpo, J. J.; Wyatt, J. R.; Dunlap, B. I. Phys. Rev. Lett. 1981, 47, 1046.
29. Olthoff, J. K.; Honovich, J. P.; Cotter, R. J. Anal. Chem. 1987, 59, 999.
30. McCreery, D. A.; Gross, M. L. Anal. Chim. Acta 1985, 178, 105.

31. Heinen, H. J. Fresenius Z. Anal. Chem. 1981, 308, 290.
32. Rollgen, F. W.; Giessmann, V. Org. Mass Spectrom. 1976, 11, 1094.

**SECTION II. ION ASSOCIATION
BY TIME-OF-FLIGHT MASS SPECTROMETRY**

ION ASSOCIATION BY TIME-OF-FLIGHT MASS SPECTROMETRY

L. Q. HUANG, R. J. CONZEMIUS, G. A. JUNK AND R. S. HOUK

AMES LABORATORY-USDOE AND DEPARTMENT OF CHEMISTRY

IOWA STATE UNIVERSITY

INTRODUCTION

Interest in time-of-flight mass spectrometry (TOF-MS) has been renewed recently (1,2) and a number of desorption ionization methods have made it especially attractive as a high mass analyzer, including ^{252}Cf plasma desorption (PDMS) (3), pulsed secondary ion mass spectrometry (SIMS) (4), and pulsed laser desorption (LD) (5). Other advantages that account for increasing interest in TOF-MS have been addressed (6).

One unique feature of TOF-MS is its ability to record a major fraction of the ions produced from a pulsed ion source. The entire mass spectrum is also recorded within a few μs . In general, TOF spectra are recorded by signal averaging or time bin averaging (7,8) to enhance the signal to noise ratio (S/N). Another unique data acquisition system for ^{252}Cf -PDMS (9) utilizes computer intelligence to sort and make decisions as information is transmitted from the mass spectrometer. This PDMS system can also record the data in such a manner that the information from each individual spectrum is available for later inspection.

Due to interests in the characterization of nonvolatile high molecular weight solid specimens including molecular speciation in the solid as well as dealing with complex mixtures such as in natural materials, we have initiated studies in LD-TOF-MS (6). The TOF-MS was designed specifically to allow the investigation of the information available from the individual TOF spectra, i.e., the study of ion association such as any co-desorption of different ion species owing to their chemical association, or ion formation from common precursors.

Some specific steps were taken to permit these studies. First, a low power, very short duration laser ion source (300ps, 10 μ J) was used to produce only a few ions per shot. With fewer ions per shot we could observe ion associations from individual mass spectra which might otherwise be masked when the number of ions-per-pulse was very high as in most ion sources for TOF-MS. Second, a data acquisition system has been developed that allows convenient recording of individual spectra for subsequent study of the differences and similarities (10). Third, classical statistical methods were used to treat the data for the study of ion association.

Here we describe the approach and report the results of ion association for the LD-TOF-MS spectra of CsI and a superconducting sample, YBa₂Cu₃O₇.

EXPERIMENTAL

The LD-TOF-MS system for this study was constructed locally and has been described (6).

Data Acquisition

The data acquisition system was designed and assembled using commercially available microelectronic components (10). Figure 1 outlines schematically how the individual spectrum from each laser shot was recorded. This technique is similar in concept but different in detail to that of Macfarlane (9). A photodiode detected the laser pulse and provided a precise time marker (t_0) for the laser desorption. This electronic pulse also started the clock of the time-to-digital convertor (TDC) which is a time interval meter capable of measuring the times of eight stop events with a resolution and accuracy of 1 ns. After ionization, the ions were accelerated to 5 kV followed by a free flight of 120 cm. Each ion was sensed by a microchannel plate detector (MCPD) which initiated an electronic pulse that was precisely synchronized with the arrival time of the ion. When these electronic pulses from the MCPD entered the TDC, the clock circuitry of the TDC performed two tasks: it determined whether this was the first, second, third or nth ion to be detected from the current laser excitation and recorded the time of arrival relative to t_0 . Ion pulses beyond the first eight were ignored.

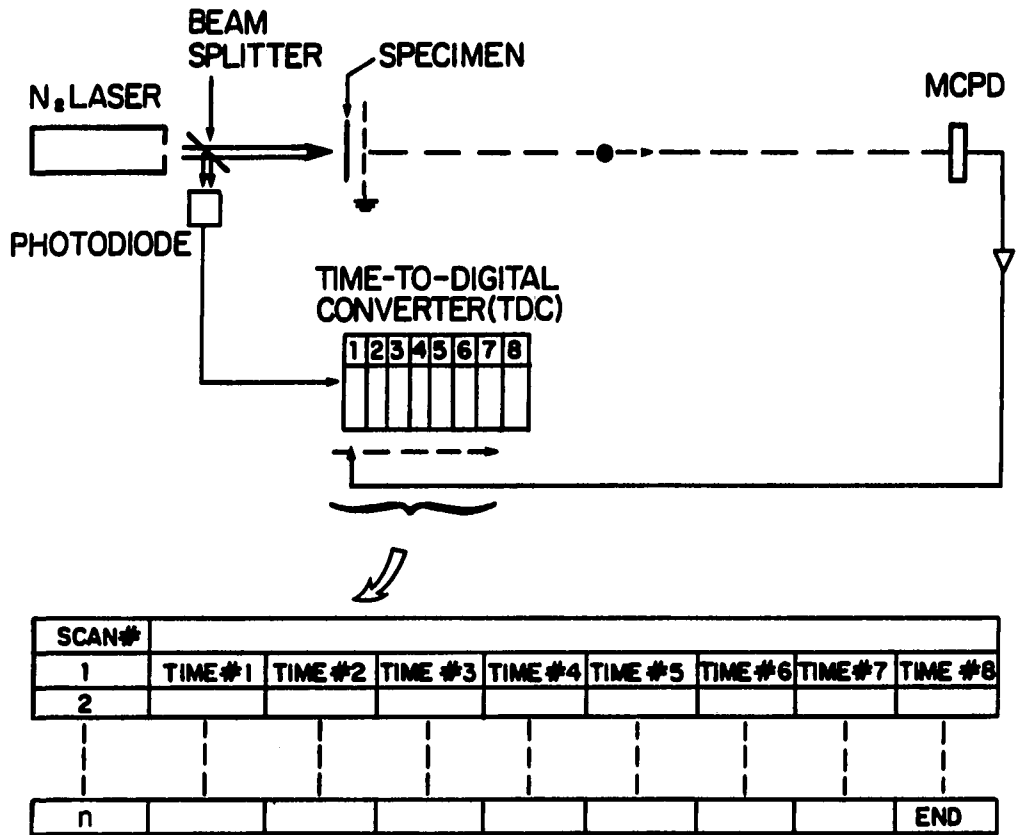


Figure 1. Schematic diagram of experimental data flow

The contents of the TDC for each laser shot (up to eight ions) were stored separately in a computer. The device can record up to one million individual spectra, although only 1000 to 2000 individual spectra were utilized for the current study.

Sample Preparation

Samples of cesium iodide were simply deposited onto a thin gold layer (50 nm thick) coated onto a quartz plate (6). The superconducting sample was ground to fine powder (400 mesh). Approximately 1 μg of the powder was carefully transferred to the center of the gold layer. A drop of deionized water was added to the powder and it was then dried for ~10 min. The water facilitated adhesion of the powder to the gold film and most of the particles adhered to the surface forming a layer ~ 20 μm thick.

DATA TREATMENT

Multiplicity Measurement

The number of ions received at the detector for an individual spectrum has been called the multiplicity (9,11). The multiplicity varies from zero to eight in this experiment.

Multiplicity can also be computed for individual spectra which contained certain ions (or for which selected ions were absent). Indeed any criterion can be applied and the result of such a computation is herein called specific multiplicity. Thus the specific multiplicity gives some indication of the tendency for the numbers of ions produced in the source to be dependent upon the selected criterion.

Ion Association Measurement

The main parameter of interest here is the tendency for one ion species, x, to be observed in certain spectra only when another ion, y, is also present, i.e., they are associated other than in a random manner.

This association can be tested by various statistical treatments such as the chi-squared (χ^2) test. The computation is conveniently expressed in a 2x2 contingency table:

	Ion y absent	Ion y present
Ion x absent	a	b
Ion x present	c	d

Where a = the number of spectra where neither ion is observed

b = the number of spectra where only ion y is observed

c = the number of spectra where only ion x is observed

d = the number of spectra where both ions are observed

The value of χ^2 is:

$$\chi^2 = \frac{n (ad - bc)^2}{(a + b) (a + c) (b + d) (c + d)} \quad (n \text{ is the number of spectra})$$

These values are compared to a standard table (see Appendix A) for confidence in the interdependence test (13). The magnitude of χ^2 value grows with the number of spectra for which the events are both present or both absent, and the denominator provides a normalizing factor. A confidence level of 99.95% was chosen in this study. Thus the association of a tested pair of ions is indicated when a computed χ^2 value is larger than 12.1.

One advantage of this test is that χ^2 differs greatly for associated or unassociated pairs, thus allowing a high confidence level such as 99.95%. Also, there are no other assumptions made as long as the observations are independent. The disadvantage of χ^2 testing is the neglect of more than one ion for the same mass detected at slightly different times in the same spectrum, but this is not a major problem in

this study because ionization conditions were selected to provide only a few ions per laser shot.

Another useful statistical treatment involves the computation of a correlation coefficient (14), γ , which tests the probability for the simultaneous occurrence for two different ion species in recurrent spectra (14):

$$\gamma = \frac{\sum_{i=1}^n (x_i - \bar{X}) (y_i - \bar{Y})}{\left(\sum_{i=1}^n (x_i - \bar{X})^2 \sum_{i=1}^n (y_i - \bar{Y})^2 \right)^{1/2}}$$

Where x_i and y_i = the number of ions x and y registered in the ith spectrum.

\bar{X} and \bar{Y} = the means of ions x and y in overall spectra.

n = the total number of observations.

Here \bar{X} is the tendency or probability for ion x to be observed; it is really just an intensity, i.e., $\bar{X} * n = \sum_{i=1}^n x_i$. Likewise for \bar{Y} . The term $\sum_{i=1}^n (x_i - \bar{X}) (y_i - \bar{Y})$ is the tendency for x_i and y_i to appear in the same observation, i.e., if $(x_i - \bar{X})$ is high while $(y_i - \bar{Y})$ is low the sum will be low and vice versa. If both terms are high in the same observations the sum grows and this tendency indicates an association (i.e., a correlation) between x and y. The denominator again provides a normalizing factor.

In effect, the correlation coefficient shows that the arithmetic average of the tendency must approach the geometric average of the

tendency when the association is present. Thus, unassociated ions would give a small of γ value approaching zero. A correlation coefficient of 1 would indicate perfect association, i.e., complete confidence in association of occurrences if a reasonably large number of spectra are tested. The computed γ for a tested pair is compared to a critical value of γ_0 from a statistical table at a chosen confidence level (13). For purposes of this study, two ions are considered associated if γ is larger than γ_0 at the 85% confidence level. The critical values for different confidence levels of the correlation coefficient are given in Appendix B.

The usage of the correlation coefficient is well accepted in scientific literature and is easily understood. Furthermore, the computation of the correlation coefficient considers the arrival of more than one ion at the same nominal mass within the same spectrum. The major limitation of the method lies in the assumption that the multiplicity follows a normal distribution which may not be true for a very low current ion source.

The optimum choice of statistical treatment depends upon ion production, i.e., the ion source, the sample, and the means of ionization. The two methods used here provide a cross reference, allowing additional confidence in the ion association measurements.

RESULTS AND DISCUSSION

General Observation of Summed TOF Spectra

The summed LD-TOF-MS spectrum of a high-temperature superconductor, $\text{YBa}_2\text{Cu}_3\text{O}_7$, is given in Figure 2, and the spectrum of CsI is shown in Figure 5 in Section I. The spectra are the summed results for 2000 individual spectra of CsI and 1000 of $\text{YBa}_2\text{Cu}_3\text{O}_7$ so that the spectra are collective information.

Cesium iodide is a good case study for ion association because of previous extensive research concerning cluster formation (11,15,16). The CsI spectrum in Figure 5 of Section I is similar to that reported by others (11) in that the $[(\text{CsI})\text{Cs}]^+$ peak is most intense followed by higher mass cluster peaks $[(\text{CsI})_n\text{Cs}]^+$ of much lower intensity. The decrease in intensity with the increase of n indicates that clusters formed by the addition of CsI molecules to these structures were evidently suppressed, either in the production process or through instability (11).

There has recently been an intense effort to investigate the phenomenon of high-temperature superconductivity (16,17). However, as yet very few analytical techniques have been applied to characterization of these materials for such properties as speciation, stoichiometry, bonding order and strength, impurities, etc. In particular we are not aware of any mass spectrometric method being applied. Hence the LD-TOF-MS spectrum in Figure 2 is of considerable interest.

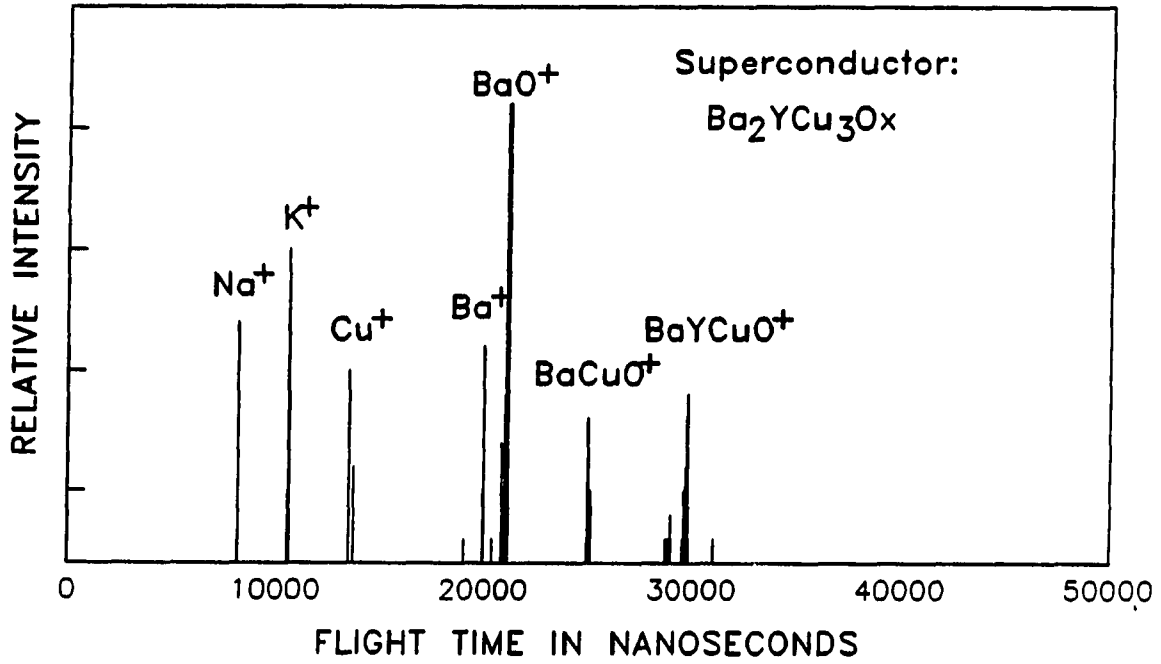


Figure 2. Summed LD-TOF-MS spectrum of $\text{YBa}_2\text{Cu}_3\text{O}_7$. The height of the BaO^+ peak is 21 counts

The overall spectrum shows the presence of Ba, Y, and Cu in the superconducting material mass spectrometrically for the first time. The molecular ions of BaO^+ , $BaCuO^+$, and $BaYCuO^+$ are detected with relatively high abundance and likely indicate stability of these molecular arrangements in the gas phase and possible also in the solid state. The alkali ions, Na^+ and K^+ , could be impurities in the sample but are more likely from the substrate since they are frequently observed in LD spectra. Other unidentified, low abundance peaks may be caused by impurities. Some surprising observations are also present. For example, Y^+ is not detected but Cu^+ and Ba^+ show a reasonable abundance. Furthermore, CuO^+ and YO^+ are not observed but BaO^+ is the most abundant ion in the spectrum.

General Observation of Individual TOF Spectra

Some individual TOF spectra for the $YBa_2Cu_3O_7$ sample are shown in Figure 3. These are spectrum numbers 135, 141, 148, 150, 180, 277, 919, and 989, respectively and are typical of the 1000 individual spectra recorded for this sample. It should be noted that there is no relative intensity in the individual spectra, i.e., the intensity is either one or zero, one meaning that an ion was detected at a specific time. A line is situated along the horizontal axis to indicate the arrival time of the ion. One percent of the spectra for CsI and sixty nine percent of spectra for $YBa_2Cu_3O_7$ contained no ions. The observation of zero ions in many spectra is not surprising and in fact is desired for the study of ion association. Approximately one percent of spectra for both

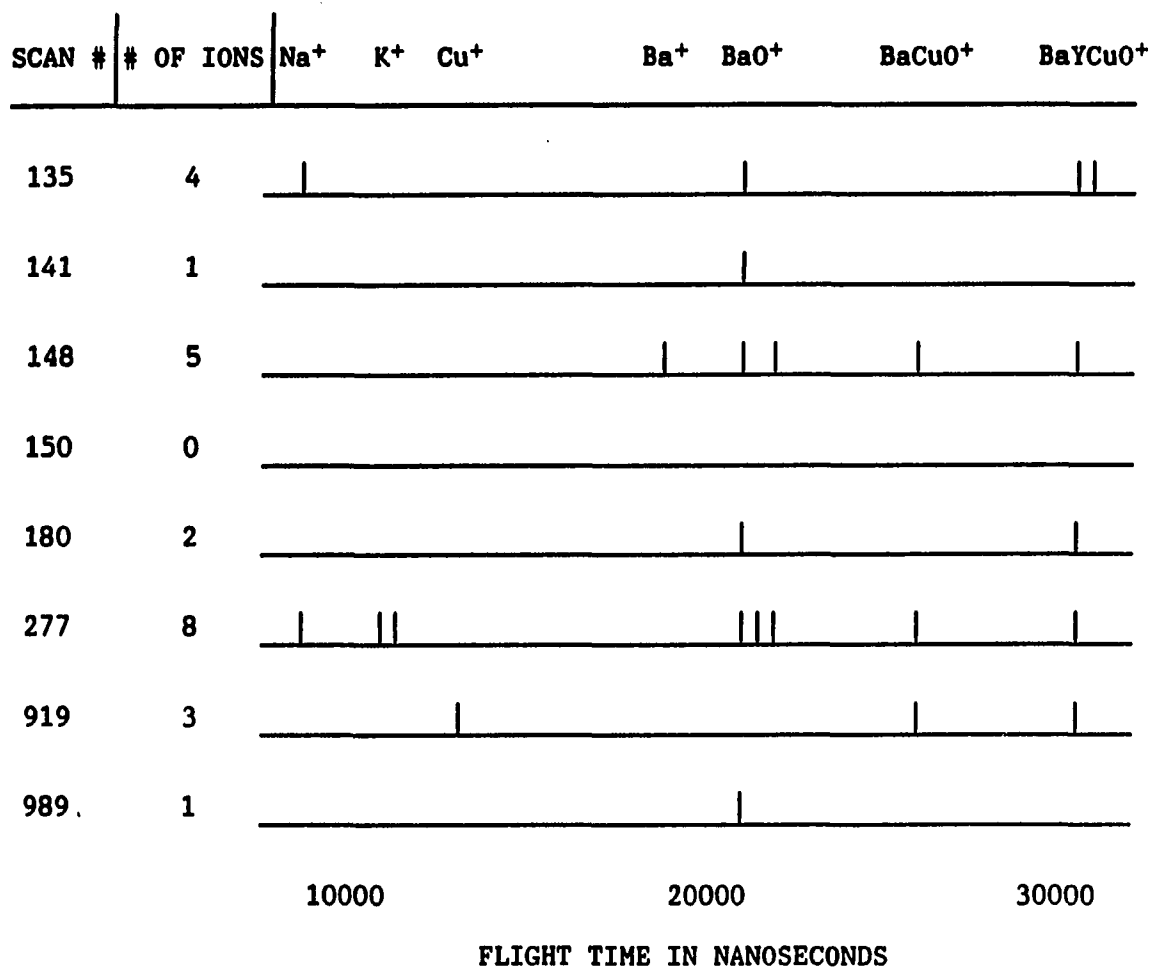


Figure 3. Illustration of selected individual TOF spectra of $\text{YBa}_2\text{Cu}_3\text{O}_7$

compounds recorded the arrival of eight ions which infers that possibly more than eight ions may have reached the detector since the TDC used here can accept only up to eight stops. It is also true that more than one ion for the same nominal mass (multiple counts) were occasionally observed in the same spectrum (e.g., peaks for BaO^+ in spectrum 148 and 277 in Figure 3). The dead time for the recording of such multiple arriving ions is 5 ns. Finally it should become apparent in viewing Figure 4 that the individual mass spectra are quite different. These differences are of primary interest here, and are due to random ion production and also to non-random ion production which is caused by properties of interest in the specimen.

Study of Multiplicity

The multiplicity distributions for individual TOF spectra for the CsI specimen and the $YBa_2Cu_3O_7$ are shown in Figures 4 and 5. Although these spectra were obtained using the same experimental conditions, the most probable multiplicity was 3 for CsI as compared to 1 (i.e., ignoring spectra with zero ions) for $YBa_2Cu_3O_7$. The efficiency of ion transmission from the ion source to the detector for this TOF-MS is at best only 50% (19) due to the transmission losses from grids and to the efficiency of the microchannel plate detector. Therefore, the actual number of ions per laser shot is higher than shown here. The obvious cause of the difference in the multiplicity distribution between CsI and $YBa_2Cu_3O_7$ is due to lower ion production in the latter case. In

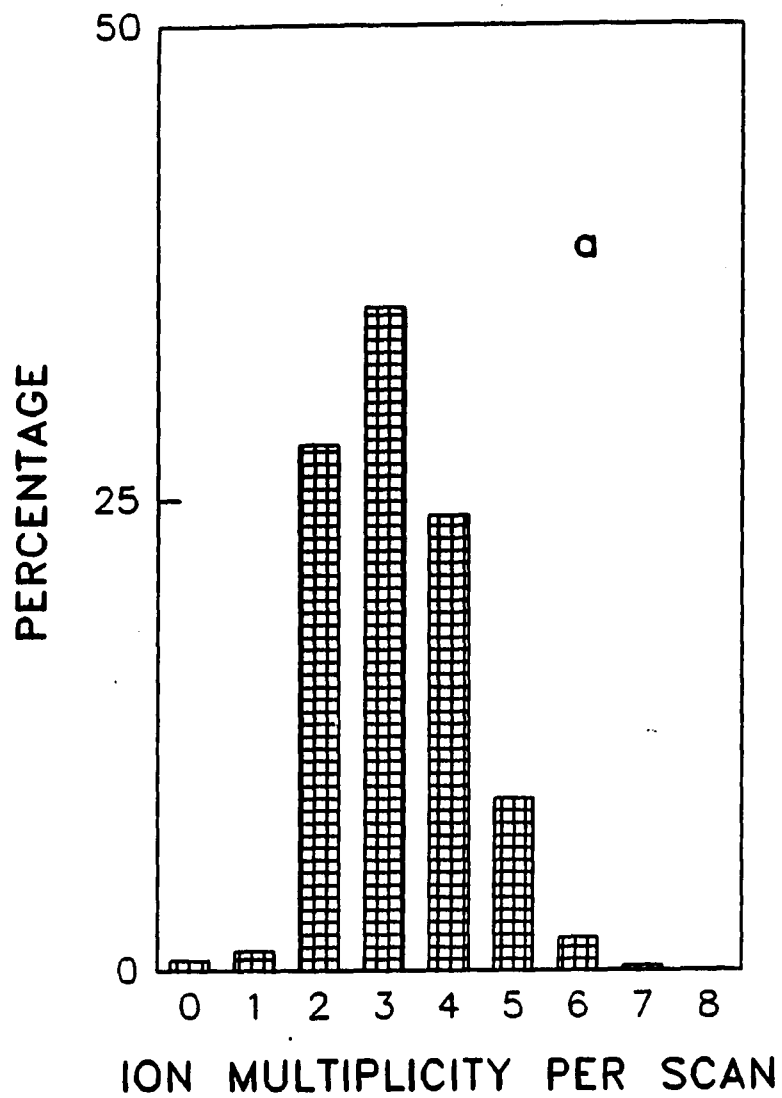


Figure 4a. Multiplicity distribution for CsI

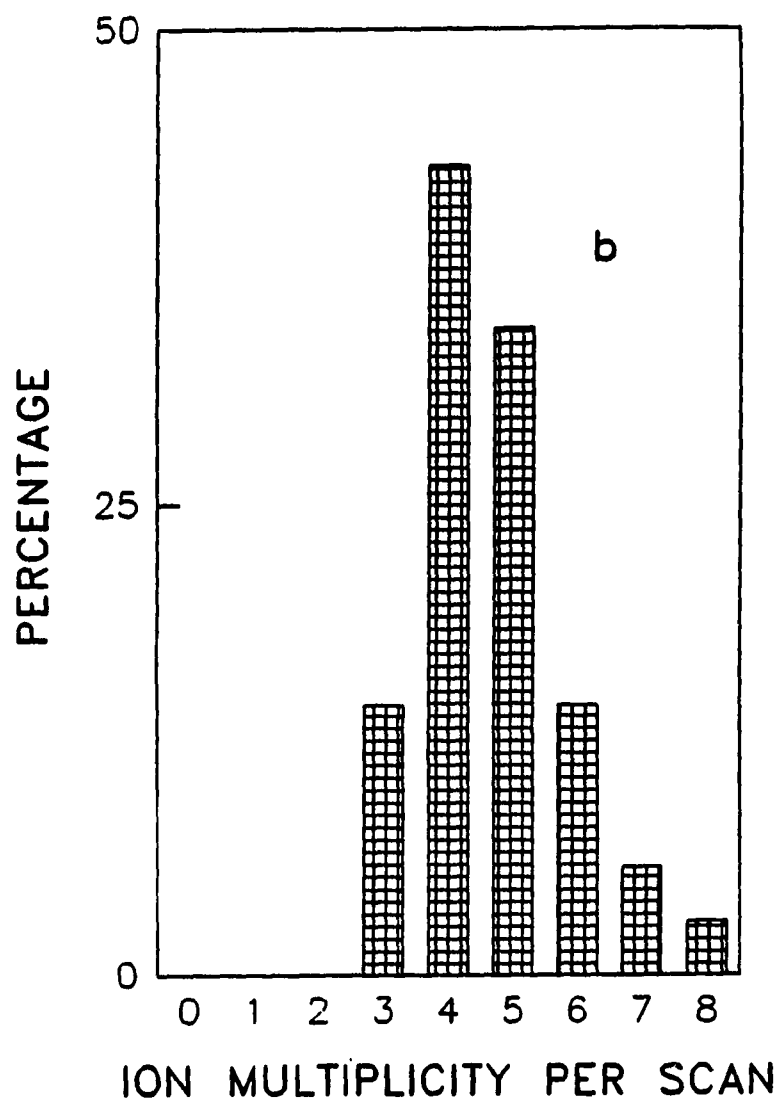


Figure 4b. Specific multiplicity distribution of spectra where the $[(\text{CsI})_2\text{Cs}]^+$ is present (~ 25% of the total spectra)

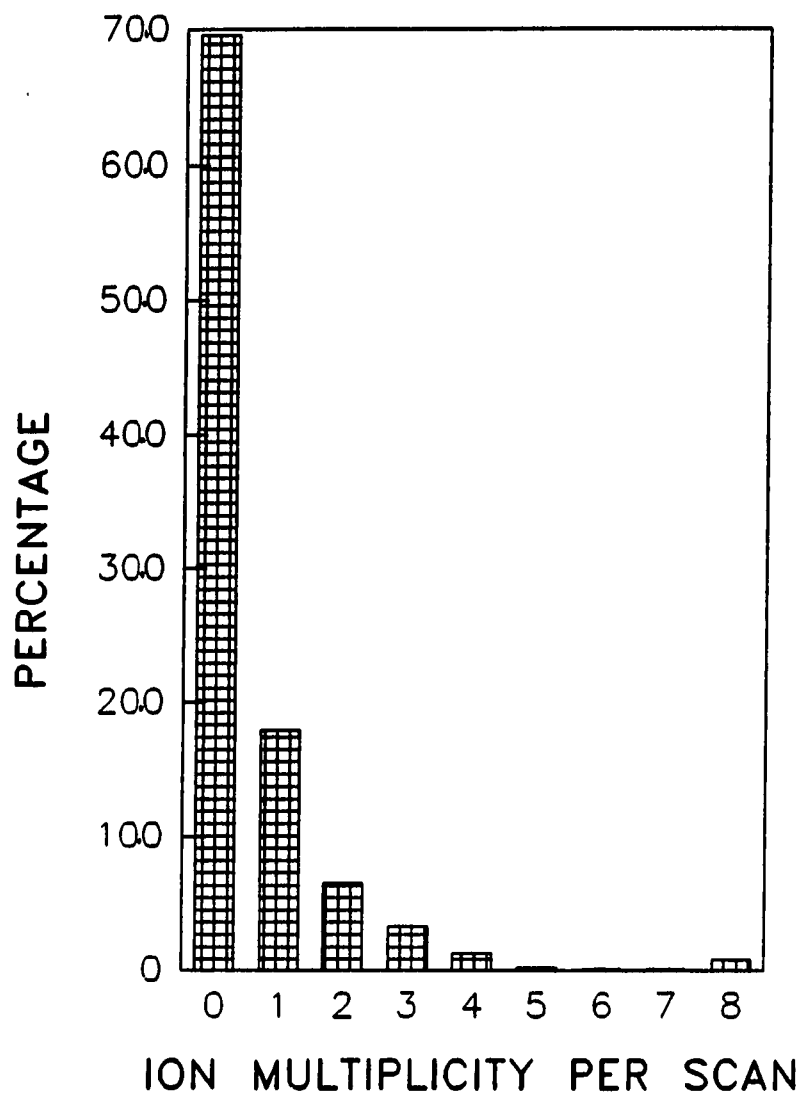


Figure 5. Multiplicity distribution for $\text{YBa}_2\text{Cu}_3\text{O}_7$

general, desorption techniques yield higher ion signals when structures in the specimen exist as "preformed ions". This may account for the higher CsI ion signal.

Figure 4b gives the specific multiplicity distribution when the ion $[(\text{CsI})_2\text{Cs}]^+$ is present in the spectrum and all other spectra are rejected. It is interesting to note that the most probable multiplicity is 4 instead of 3 in Figure 4a and that the percentages of 1 and 2 are zero in this distribution. A possible explanation is that low mass ions such as Cs^+ or $[(\text{CsI})\text{Cs}]^+$ participate in the formation of massive cluster ions in the gas phase or selvedge reactions between co-desorbing particles. Thus such cluster ions would be observed only from shots for which the gas phase is more dense, and the resulting spectra would have higher specific multiplicity.

Study of Ion Association

The results of ion association tests for the CsI sample are given in Tables 1 and 2. Both data treatments indicate that Cs^+ and $[(\text{CsI})\text{Cs}]^+$ are associated but not other ion pairs. Although the χ^2 test indicates marginal confidence in association between $[(\text{CsI})\text{Cs}]^+$ and $[(\text{CsI})_2\text{Cs}]^+$, the correlation coefficient shows no association for this pair. The conflict in these tests for association is likely affected by a high percentage of multiple counts for the same mass which are not accounted for in the χ^2 test.

The observation of ion association between Cs^+ and the $[(\text{CsI})\text{Cs}]^+$ but not between any other ion pairs in the CsI spectrum infers that Cs^+

Table 1. Results of 2x2 Contingency Table Test of Ion Association for LD-TOF Mass Spectra of CsI

Tested Pairs	χ^2	Associated
Cs ⁺ & [(CsI)Cs] ⁺	64.363	Yes
Cs ⁺ & [(CsI) ₂ Cs] ⁺	0.115	No
Cs ⁺ & [(CsI) ₃ Cs] ⁺	0.916	No
[(CsI)Cs] ⁺ & [(CsI) ₂ Cs] ⁺	10.090	No
[(CsI)Cs] ⁺ & [(CsI) ₃ Cs] ⁺	0.221	No
[(CsI) ₂ Cs] ⁺ & [(CsI) ₃ Cs] ⁺	1.278	No

Table 2. Correlation Coefficients (γ) for TOF Spectra
of CsI

Tested Pairs	Computed γ	Associated
Cs ⁺ & [(CsI)Cs] ⁺	0.2060	Yes
Cs ⁺ & [(CsI) ₂ Cs] ⁺	0.03508	No
Cs ⁺ & [(CsI) ₃ Cs] ⁺	0.00624	No
[(CsI)Cs] ⁺ & [(CsI) ₂ Cs] ⁺	0.02029	No
[(CsI)Cs] ⁺ & [(CsI) ₃ Cs] ⁺	0.04389	No
[(CsI) ₂ Cs] ⁺ & [(CsI) ₃ Cs] ⁺	0.02809	No

and the [(CsI)Cs]⁺ may have a commonality in the formation process not present for the other polymer ions (13). This commonality may account for the extraordinarily high intensity of the monomer but very low intensity for the polymers in the conventional spectrum. Here the particle density in the selvedge region was considered to be very low for three reasons. First, the energy input to the specimen is made as low as possible while still retaining detectable ion emission. Second, little latent ion emission from the surface was observed (6) which indicated that prompt emission was the primary means of ion production. Third, the TOF ion source design allowed very short times (~ 40 ns) between ion production and acceleration into the vacuum region.

Tables 3 and 4 show the test results of ion association for the YBa₂Cu₃O₇ sample. Both statistical criteria indicate association between the following pairs: Ba⁺ and BaO⁺, BaO⁺ and BaCuO⁺, BaO⁺ and BaYCuO⁺, BaCuO⁺ and BaYCuO⁺, but not for other ion pairs. In fact, the plot of χ^2 values vs γ values in Figure 6 for these four pairs shows a roughly linear relationship indicating that the two data treatments yield similar conclusions about association for these ion pairs.

The chemical basis for these ion associations should be relevant for this material. There is evidence that YBa₂Cu₃O₇ undergoes slow decomposition at room temperature in the presence of water to produce oxides of copper and barium (20). It is reasonable to assume that BaO⁺ was produced from both the superconducting crystal and the barium oxide present due to prior decomposition. BaO⁺ (emitted from crystal), BaCuO⁺, and BaYCuO⁺ are likely associated with each other since they are

Table 3. Results of 2x2 Contingency Table Test of Ion Association for LD-TOF Mass Spectra of YBa₂Cu₃O₇

Tested Pairs	χ^2	Associated
Cu ⁺ & Ba ⁺	0.212	No
Cu ⁺ & BaO ⁺	0.209	No
Cu ⁺ & BaCuO ⁺	0.170	No
Cu ⁺ & BaYCuO ⁺	0.243	No
Ba ⁺ & BaO ⁺	37.50	Yes
Ba ⁺ & BaCuO ⁺	6.709	No
Ba ⁺ & BaYCuO ⁺	0.017	No
BaO ⁺ & BaCuO ⁺	18.70	Yes
BaO ⁺ & BaYCuO ⁺	14.40	Yes
BaCuO ⁺ & BaYCuO ⁺	17.70	Yes

Table 4. Correlation Coefficients (γ) for TOF Spectra
of Superconductor, $\text{YBa}_2\text{Cu}_3\text{O}_7$

Tested Pairs	Computed γ	Associated
Cu^+ & Ba^+	0.04296	No
Cu^+ & BaO^+	0.05246	No
Cu^+ & BaCuO^+	0.05146	No
Cu^+ & BaYCuO^+	0.07677	No
Ba^+ & BaO^+	0.2147	Yes
Ba^+ & BaCuO^+	0.05007	No
Ba^+ & BaYCuO^+	0.01892	No
BaO^+ & BaCuO^+	0.1530	Yes
BaO^+ & BaYCuO^+	0.1093	Yes
BaCuO^+ & BaYCuO^+	0.1251	Yes

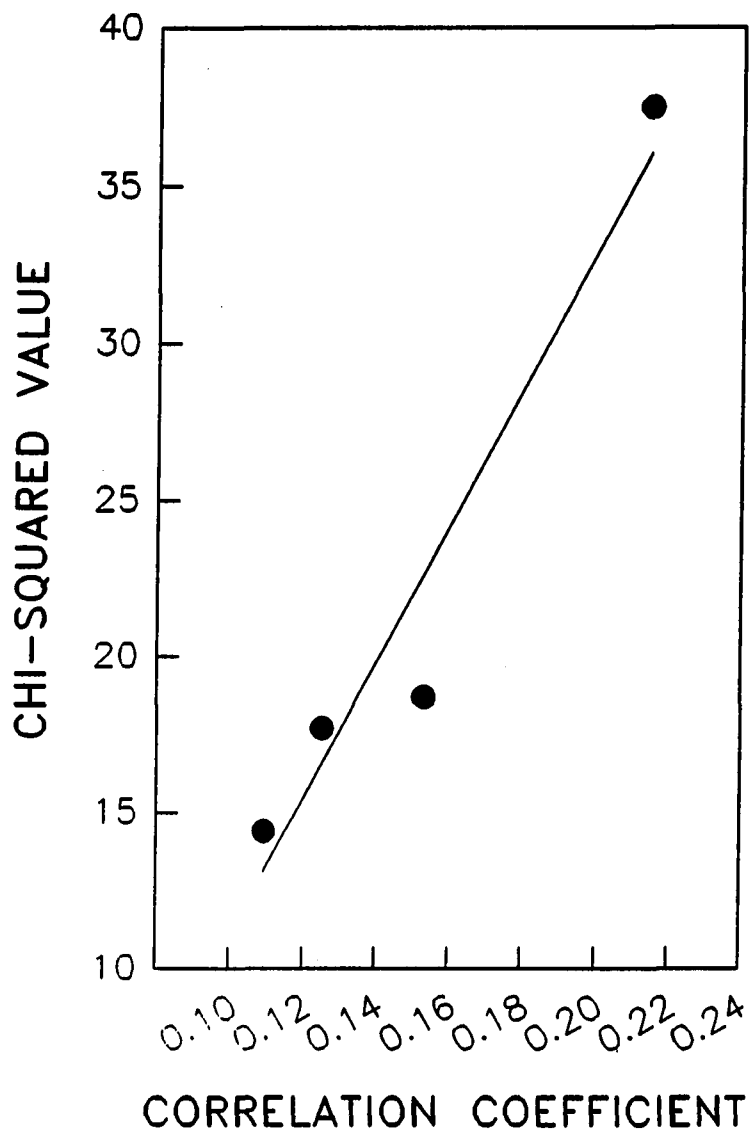


Figure 6. Plot of chi-squared values (χ^2) vs. correlation coefficient (γ) for four associated ion pairs in $\text{YBa}_2\text{Cu}_3\text{O}_7$

produced from the same phase. The Ba^+ ion is likely associated with BaO^+ because they are also produced from the same solid phase - the barium oxide present from the decomposition. These Ba^+ ions are not likely to be produced directly from the superconducting crystal so one would not expect association of Ba^+ with $BaCuO^+$ and $BaYCuO^+$. Similar arguments can be made for the presence of Cu^+ ions being due to a CuO phase in the specimen. These arguments agree with the notion that laser desorption should not produce elemental ions directly from the superconductor matrix due to the nature of "soft-ionization" causing minimum fragmentation (6). Thus, perhaps no singly charged yttrium ions are detected because no yttrium oxide is present. Barium oxide ($\Delta H_f^0 = -123.8 \text{ KJ mol}^{-1}$) is much more stable than copper oxide ($\Delta H_f^0 = 306.3 \text{ KJ mol}^{-1}$) in the solid state, providing a basis for explaining why CuO^+ is not observed while BaO^+ ions have the highest intensity.

SUMMARY AND CONCLUSION

The study of ion association from individual TOF spectra provides useful information for both fundamental studies and analytical applications. The two statistical approaches applied here can be used profitably in TOF-MS where ion currents are purposely kept low such as dynamic TOF SIMS or in other mass spectrometers capable of detecting all ions from pulsed ionization such as Fourier transform mass spectrometers. Clearly the investigation of individual TOF spectra provides a "microscopic" view of single ionization processes so that much more information is available. This added parameter or resolution element can greatly increase the informing power of the analytical technique. The associations should be better understood when better control of ion current sources is realized. Applications of these associations should be expanded when organic and biochemical specimens are examined in future studies.

The direct analysis of superconducting materials with MS is especially pertinent. In future studies, LD-TOF-MS is expected to provide at least "finger-print" information from calibrations with known specimens to allow confirmation or comparison of new superconductor spectra which otherwise appear identical. Ion association studies in LD-TOF-MS may also be useful in monitoring the presence of second phases or altered stoichiometry both of which greatly affect superconductivity.

We expect the concept of ion association to become a standard feature in time-of-flight mass spectrometry.

LITERATURE CITED

1. Knorr, F. J.; Ajami, M.; Chatfield, D. A. Anal. Chem. 1986, 58, 690.
2. Borman, S. Anal. Chem. 1987, 59, 701A.
3. Macfarlane, R. D.; Torgerson, D. F. Int. J. Mass. Spectrom. Ion Phys. 1976, 21, 81.
4. Chait, B. T.; Standing, K. G. Int. J. Mass. Spectrom. Ion Phys. 1981, 40, 185.
5. Hillenkamp, F. "Ion Formation from Organic Solids", Benninghoven, A. Ed.; Springer-Verlag: Berlin, 1983; Vol. 25, P. 190.
6. Huang, L. Q.; Conzemius, R. J.; Junk, G. A.; Houk, R. S. Anal. Chem. Submitted, 1987.
7. Holland, J. F.; Enke, C. G.; Allison, J.; Stults, J. T.; Pinkston, J. D.; Newcome, B.; Watson, J. T. Anal. Chem. 1983, 55, 997A.
8. Holland, J. F.; Erickson, E.; Eckenrode, B. A.; Watson, J. T.; Presented at 35th Conference of the American Society for Mass Spectrometry, Denver, Colorado, 1987.
9. Macfarlane, R. D. Anal. Chem. 1983, 55, 124A.
10. Conzemius, R. J.; Aducci, D.; Huang, L. Q.; Junk, G. A.; Houk, R. S. Department of Chemistry, Iowa State University; to be published.
11. Ens, W. Ph.D. Dissertation, University of Manitoba, Manitoba, Canada, 1982.
12. Kendall, M. G.; Stuart, A. "The Advanced Theory of Statistics", 4th ed.; Charles Griffin & Company LTD: London, 1979; Vol. 2, Chapter 13.

13. Neave, H. R. "Statistics Tables"; George Allen and Unwin: Boston, 1978; P. 58.
14. Snedecor, G. W.; Cochran, W. G. "Statistical Methods", 7th ed.; Iowa State University Press: Ames, Iowa, 1980; Chapter 10.
15. Campana, J. E.; Barlak, T. M.; Colton, R. J.; Decorpo, J. J.; Wyatt, J. R.; Dunlap, B. I. Phys. Lett. 1981, 47, 1046.
16. Campana, R. J. Mass. Spectrom. Rev. 1987, 6, 395.
17. Bednorz, J. G.; Mueller, K. A. Z. Phys. B 1986, 64, 189.
18. Wu, M. K.; Ashburn, J. R.; Torng, C. T.; Hor, P. H.; Meng, R. L. Huang, Z. J.; Wang, Y. Q.; Chu, C. W.; Phys. Rev. Lett. 1987, 58, 908.
19. Brunnee, C. Int. J. Mass Spectrom. Ion Processes 1987, 76, 121.
20. McCarley, R. E. Department of Chemistry, Iowa State University, Private Communication, 1987.

**SECTION III. REDUCTION OF SIGNAL REFLECTION
FOR RECORDING FAST PULSES FROM A MICROCHANNEL PLATE DETECTOR**

REDUCTION OF SIGNAL REFLECTION FOR RECORDING

FAST PULSES FROM A MICROCHANNEL PLATE DETECTOR

L. Q. HUANG, R. J. CONZEMIUS, G. E. HOLLAND AND R. S. HOUK

AMES LABORATORY-USDOE AND DEPARTMENT OF CHEMISTRY

IOWA STATE UNIVERSITY

INTRODUCTION

Microchannel plate detectors (MCPD) have been widely used in nuclear sciences, physics, and military applications (1-4) because of their high spatial resolution, ruggedness, and sensitivity. In recent years, MCPDs have also gained popularity in mass spectrometry (5), particularly in time-of-flight mass spectrometry (TOF-MS). TOF-MS requires a detector yielding an output signal with high speed (risetime of 1 ns), high gain, low noise, and a large ion collection area (e.g., several cm^2). The ion collection area should also be a flat surface, perpendicular to the path of the arriving ions. An MCPD meets these needs.

In the development of a TOF-MS (6), it is useful to place the ion detector in different locations along the ion flight path for various experiments. A common problem in the pulse recording mode with MCPD assembly is the reflection of signal pulses when proper precautions are not followed. This section describes techniques for attenuating signal reflections for fast pulse recording with a home-made, movable MCPD assembly and subsequent signal transmission to a high speed amplifier for a high resolution TOF-MS.

EXPERIMENTAL

Two schematic views of the MCPD mechanical arrangement are shown in Figure 1. The characteristics of the microchannel (MCP) as well as pertinent experimental parameters are given in Table 1.

Microchannel plates are normally used in tandem since two MCPs in series give the 10^6 gain needed for ion detection. The two plates were arranged such that the bias angle of the channels oppose each other as indicated in Figure 1. A 0.125 mm thick metal ring was sandwiched between the two plates for electrical contact to the inner surfaces. The two plates were then clamped between two stainless steel rings to provide mechanical support and electrical connections to the outer surfaces. The tandem assembly was mounted onto the detector housing with insulated standoffs.

Two grids were used for electrical shielding. The electron suppressor grid (tungsten, 85% transmission) was 2.5 mm above the top MCP and was held at the same negative potential as the upper surface of the top MCP. This grid prevented secondary electrons created at ion impact from being accelerated back toward the incoming beam. The grounded grid (tungsten, 85% transmission) isolated the detector mouth from the field-free region of the TOF-MS.

The electron collector (anode) was a stainless steel plate with a surface area the same as the active area of the MCP to maximize the collection efficiency of electrons. The spacing between the anode and MCP was set at 1 cm to allow high electron collection efficiency and minimize capacitive coupling to the plates. This distance gave

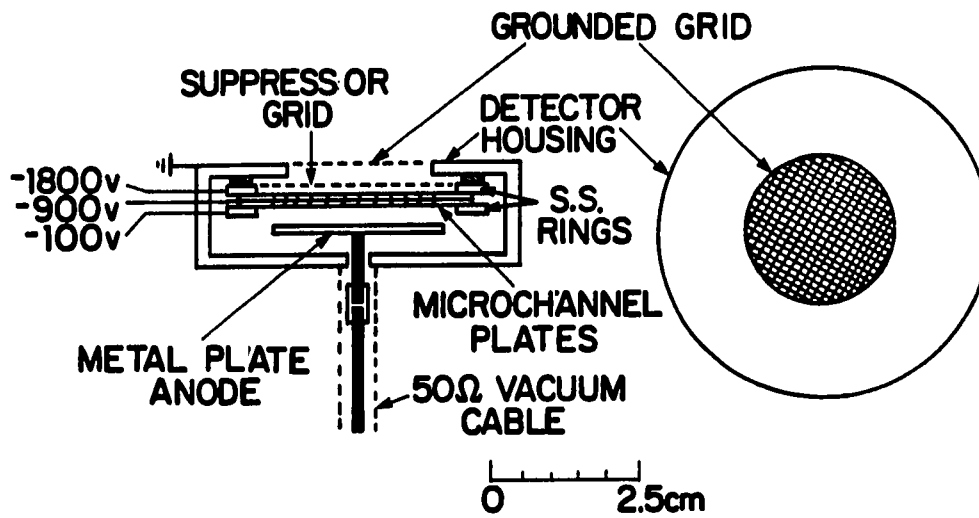


Figure 1. Two schematic views of the MCPD assembly

Table 1. Experimental Parameters

Component	Dimensions or Operating Conditions	
Microchannel plate: Varian Image Tube Division Model VUV8946	Active area Active area diameter Electron gain Plate thickness	5 cm ² 2.50 cm 8.9 x 10 ³ 0.04 cm
MCPD Assembly: Ames Laboratory construction	Assembly O. D. S. S. rings: thickness O.D. I.D. Metal anode: thickness Diam.	6.25 cm 0.25 cm 5.00 cm 2.50 cm 0.15 cm 2.50 cm
50 Ω impedance feedthrough MDC Model IF-155	O.D.	2-3/4 inch

satisfactory results (6), and thus other anode configurations were not tested.

The anode was connected to a copper rod (2 mm dia. x 2 cm long) which was mechanically supported with a Kel F ring which was press fit into the housing. The shield between the copper rod and the center wire of the 50 Ω vacuum cable (Coax Cable RG 142B/u) was carefully extended over the connector and then attached to the detector housing with a small clamp. An effort was made to retain uniform spacing between the central wire, the connector, and the copper rod to minimize distortions. A slight flaring of the shield to about 1.5x its original diameter occurred at the connection out to the detector housing. A pressure of $< 5 \times 10^{-8}$ torr was achieved before and after installation, i.e., the cable did not outgas severely.

The performance tests were made with the arrangement shown in Figure 2. The ion signal pulses, produced by a continuous ion source, were monitored with a 50 Ω terminated oscilloscope (Tektronix model 2465). The signal pulses originating directly from the MCPD were monitored at point A. Connection B allowed monitoring of the signal pulses after amplification (LeCroy Model 612AM, gain ~ 10 X).

Performance tests were also made in which the 50 Ω vacuum cable connection between the MCPD and the high frequency flange was replaced by a similar length of bare nickel wire.

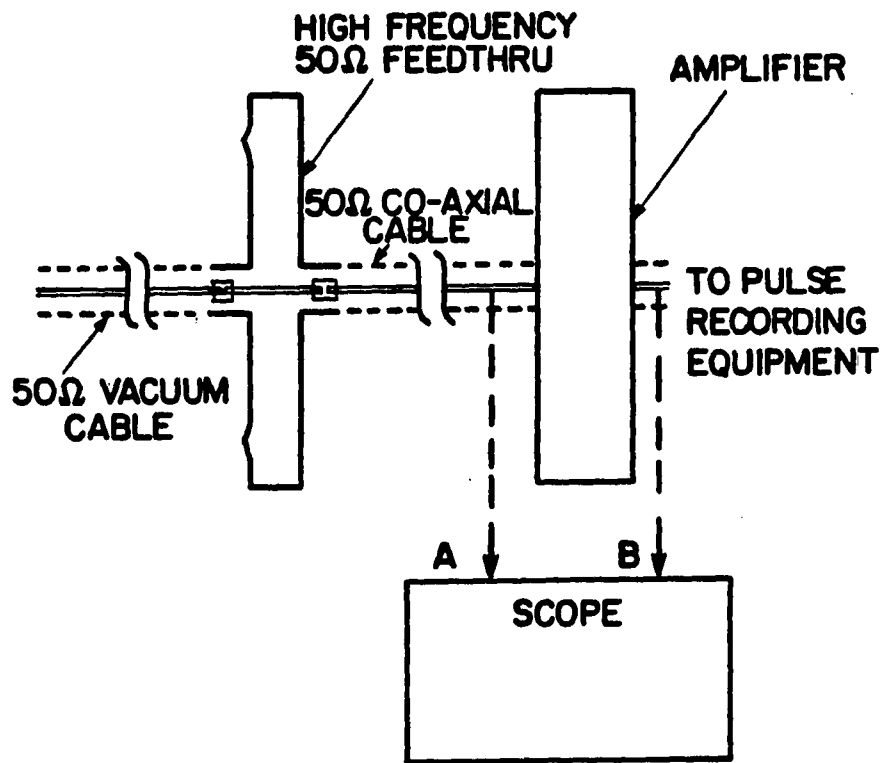


Figure 2. Performance test arrangement

RESULTS AND DISCUSSION

Distortion of transmitted pulses resulting from the reflection of signal is shown in Figure 3 when the bare nickel wire coupling was used. The reflections are of comparable amplitude to the signal pulse at about 8 ns intervals. These reflections make it difficult to set the discriminator level; they also cause poor time resolution, increased dead time, and other deleterious effects on circuits that respond to the reflected signals. These effects are illustrated in Figure 4, which shows the amplifier output. The positive reflected signal exceeds the saturation level of the amplifier. After amplification, the reflections are even closer in height to the first negative signal pulse than was the case for the direct output of the detector. The threshold level of the counting equipment cannot be set to discriminate between the main pulse and the first reflected pulse, and some of the second reflections could be counted also. This effect likely caused the artifact peaks noted in the TOF-MS experiment described in Reference (7).

Signal reflection in transmission lines is caused by improper impedance matching between the MCPD anode and the vacuum feedthrough even though proper cabling and impedance matching is used outside the housing. The effect can be described in terms analogous to light optics. The transmission of electrical pulses can be viewed as constructive and destructive interference in a standing wave within an optical cavity where the impedance match is analogous to the matching of indexes of refraction at the end of the cavity and the length of the cavity is analogous to the length of the electrical transmission line.



Figure 3. Picture of oscilloscopic display of MCPD signal pulse with an Ni wire connection. Each division on the horizontal axis represents 10 ns. Approximately 40,000 ion pulses were summed for this and subsequent Figures

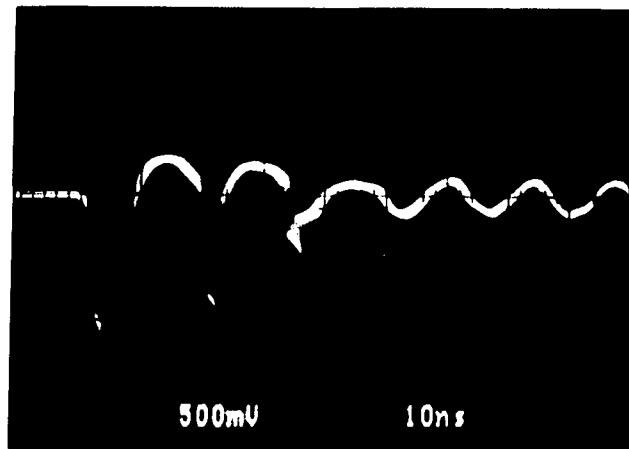


Figure 4. Picture of an oscilloscopic display of the amplified pulse from Figure 3

The velocity of propagation of the electronic pulse can be estimated from the transmission line and termination characteristics. Hence the impedance match throughout the whole transmission line is very critical, particularly for accurate transmission of a fast pulse (1 - 2 ns) obtained from a MCPD.

When the MCPD anode was connected (as shown in Figure 1 and described earlier) with 50 Ω vacuum cabling to a 50 Ω impedance matched feedthrough the reflections were virtually eliminated as shown in Figure 5. Despite the same voltage bias on the MCPD, the amplitude of the signal pulse decreased from \sim 170 mv in Figure 3 to \sim 140 mv in Figure 5, indicating an indeterminate impedance of the bare wire connection exceeding 50 Ω . The photo of the scope signal in Figure 5 was taken with an exposure time of 10 min, representing a visual summary of \sim 40,000 single ion pulses. The rise time of approximately one ns shown in Figure 5 indicates that the acceptable pulse characteristics are reproducible with a definite improvement over those in Figure 3. The fast rise time and narrow pulse width shown here have yielded good results in practical applications (6).

Figure 6 shows the signal pulse shape after amplification of the MCPD signal from Figure 5. The rise time of the amplified signal is about the same as the MCPD signal and, of course, the large reflected signals shown in Figure 4 are greatly attenuated. The standard way to minimize signal reflections and distortion in pulse counting detection is simply to keep the signal lead as short as possible (8), which means the detector must be situated close to the feedthrough flange. The

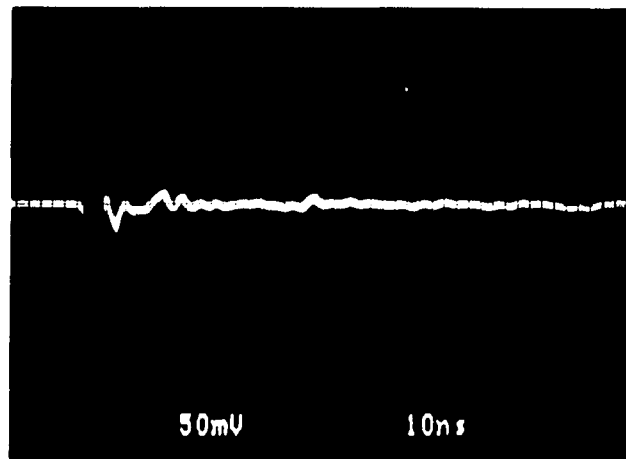


Figure 5. Picture of oscilloscopic display of the signal pulse with 50 Ω impedance matched vacuum cable connection

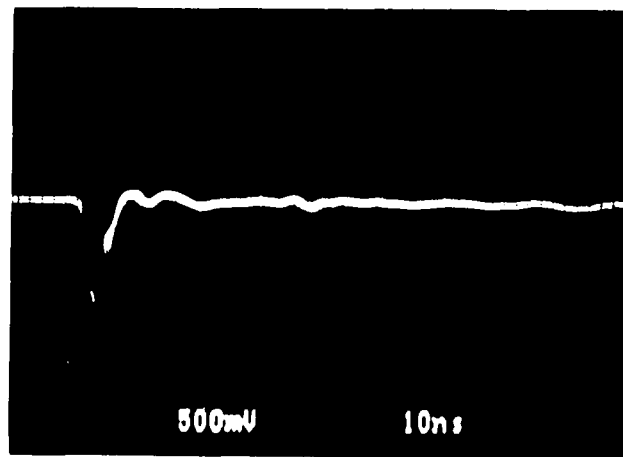


Figure 6. Picture of oscilloscopic display of the amplified pulse from Figure 5

shielding and impedance matching techniques described above permit placing the detector wherever desired within the vacuum housing, which was one objective of the present work.

SUMMARY AND CONCLUSION

The performance of a movable, home-made MCPD assembly is evaluated and found comparable to a commercial design which is mounted onto a special flange (9). A 50 Ω impedance vacuum cable coupling to a 50 Ω impedance matched feedthrough allows flexibility in research studies or in special ion optical configurations where the MCPD cannot be positioned close to a vacuum port. This flexibility becomes important as more studies in TOF-MS are performed. The MCPD assembly described here could also be adapted to the use of three microchannel plates for ion detection with high gain if desired although the effect of such use on the pulse shape is not known. Some experimental apparatus may require impedances other than 50 Ω but similar techniques can be used.

LITERATURE CITED

1. "Applications for Microchannel Plates," Varian, Palo Alto, CA; Company Report, 1982.
2. Wize, J. L. Nucl. Ins. Meth. 1979, 162, 587.
3. Bolore, M.; Girard, J. Nucl. Ins. Meth. 1977, 140, 279.
4. Gabor, G.; Schimmerling, W.; Greiner, D.; Bieser, F.; Lindstrom, P. Nucl. Ins. Meth. 1975, 130, 65.
5. Borman, S. Anal. Chem. 1987, 59, 701A.
6. Huang, L. Q.; Conzemius, R. J.; Junk, G. A.; Houk, R. S. Anal. Chem. Submitted.
7. Opsal, R. B.; Owens, K. G.; Reilly, J. P. Anal. Chem. 1985, 57, 1884.
8. Kurz, E. A. Amer. Lab. 1979, 11, 67.
9. "Application Note for the Fast Timing Detector Having A 50 Ω Co-axial Anode," Galileo Electro-Optics Corp., Sturbridge, MA; Company Report, 1986.

**SECTION IV. DIRECT DETERMINATION OF
TRACE ELEMENTS IN SOLIDS BY LASER MASS SPECTROMETRY**

**DIRECT DETERMINATION OF TRACE ELEMENTS IN SOLIDS
BY LASER MASS SPECTROMETRY**

**L. Q. HUANG, R. J. CONZEMIUS AND R. S. HOUK
AMES LABORATORY-USDOE AND DEPARTMENT OF CHEMISTRY
IOWA STATE UNIVERSITY**

INTRODUCTION

The application of laser mass spectrometry (LMS) to elemental characterization of solid materials has grown significantly in recent years (1,2). In principle, LMS can meet most of the needs for this type of analytical measurement. These needs include: 1. Little or no sample preparation. 2. Large dynamic range. 3. Provision for measuring spatially-resolved concentrations. 4. Minimal matrix and interelement effects. 5. Broad elemental coverage including interstitial impurities such as H, C, N, and O (3). 6. Isotopic information. 7. Ability to analyze insulators or semiconductors without rendering the samples conductive. An LMS system has been developed in this laboratory for elemental analysis of a wide variety of solid samples (4). For most of these samples, calibration standards are not available, so elemental concentrations are determined by comparing the m/z -resolved ion signal for an analyte element to the total ion beam signal. The assumption is generally made that the various elements are ionized in the laser mini-plasma and detected by the mass spectrometer with uniform efficiency so that calibration standards that closely match the matrix composition of the sample are unnecessary. Previous work on the determination of C, N, and O in metals indicated that this assumption yielded good accuracy ($\pm 10\%$ relative) despite the high ionization energies of these elements (3). In the present work, the uniformity of response for other impurity elements in metals is tested by analysis of standard reference materials (SRMs). Determination of trace oxygen in silicon is also investigated.

EXPERIMENTAL

The laser mass spectrometer has been described previously (4). Instrumental components and operating conditions pertinent to this study are identified in Table 1. The laser used had a long pulse width and a high repetition rate. The latter feature facilitated averaging data from many laser shots to compensate for pulse-to-pulse variations in ion production. The laser beam had a large depth-of-focus to minimize power density changes caused by variations of the sample surface relative to the focal point of the laser (5). Also, the laser beam was rastered over the surface to produce ions from a large, representative section of the sample. A glass microscope slide located approximately 2 cm from the specimen served to protect the other light transmitting components from condensation. A fresh area of the slide was moved into the beam path every 20 min. The ion kinetic energy spread transmitted by the electrostatic analyzer encompassed ~ 40% of the total ions produced in the laser microplasma. This wide energy spread acceptance by the mass analyzer minimizes discrimination in the transmission efficiency for ions at different m/z caused by differences in their kinetic energies.

The relative sensitivity factor (RSF) was used to calibrate the response of the instrument:

$$RSF = \frac{\left(\frac{I_{M^+}}{I_{total}}\right)\left(\frac{C_M}{A_M}\right)}{\left(\frac{I_{^{56}Fe^+}}{I_{total}}\right)\left(\frac{C_{Fe}}{A_{^{56}Fe}}\right)} \quad (1)$$

Table 1. Instrumental Facilities

Component	Operating Conditions
Laser	
Nd-Yag with acousto-optic Q switch. Model 255 QT. Holobeam Corp. (Acquired by Control Laser Corp.) Focused with 6.75 x upcollimator and 60 mm lens.	Wavelength 1.06 μm Pulse width (half height) 100 ns Spot size 12 μm Pulse energy 0.01 - 1.0 mJ
Mass Spectrometer	
Double focusing with Mattach-Herzog geometry Ames Laboratory construction (3)	Ion energy window \sim 150 eV m/z switched electrostatically with constant magnetic field.
Ion Source	
Ames Laboratory construction (3) Sample inserted through vacuum lock Chamber evacuated with Cryopump (Model VK-12A, Varian)	Object slit \sim 500 μm Source pressure 1×10^{-7} Torr Pumping speed 1000 Ls^{-1}
Detector	
Faraday cup signal amplified with Model 401MR, Cary Instruments (Subsidiary of Varian Corp., Monrovia, CA).	Charge measurement with internal capacitance 2×10^{-11} f
Control and Data Acquisition Computer Model LSI 11-73 Digital Equipment Corp.	TXS PLUS Operating System Details of software, interfaces, etc. available from authors.

where I_{M^+} = m/z-resolved analyte ion signal
 I_{56Fe} = iron ion signal observed
 I_{total} = total ion signal at beam monitor (4)
 C_M, C_{Fe} = concentration of analyte and Fe
 A_M, A_{56Fe} = natural abundance of analyte isotope and Fe isotope monitored.

The denominator of the above expression represents a correction for the transmission efficiency of the mass analyzer and relative detection efficiencies of the Faraday cup and the total ion beam monitor. An RSF of unity means that the analyte element was ionized and detected with the same efficiency as Fe.

Procedure

As the ion source was evacuated, the specimen was brought into coarse focus by the operator using a microscope (100x) mounted coaxially with the laser beam. The laser beam parameters, specimen position, mass spectrometer settings, and data acquisition were then controlled by a computer program (6), which had the general algorithm given in Figure 1. This control process automatically fulfilled requirements identified previously for generating a clean specimen surface (3) and for obtaining reproducible and efficient ion production (5).

The first experiment measured the influence of laser power density on RSF. The laser power density was adjusted without changing the spot diameter by varying the lamp current to the optical pump (4).

Measurements were taken at the different power densities for two

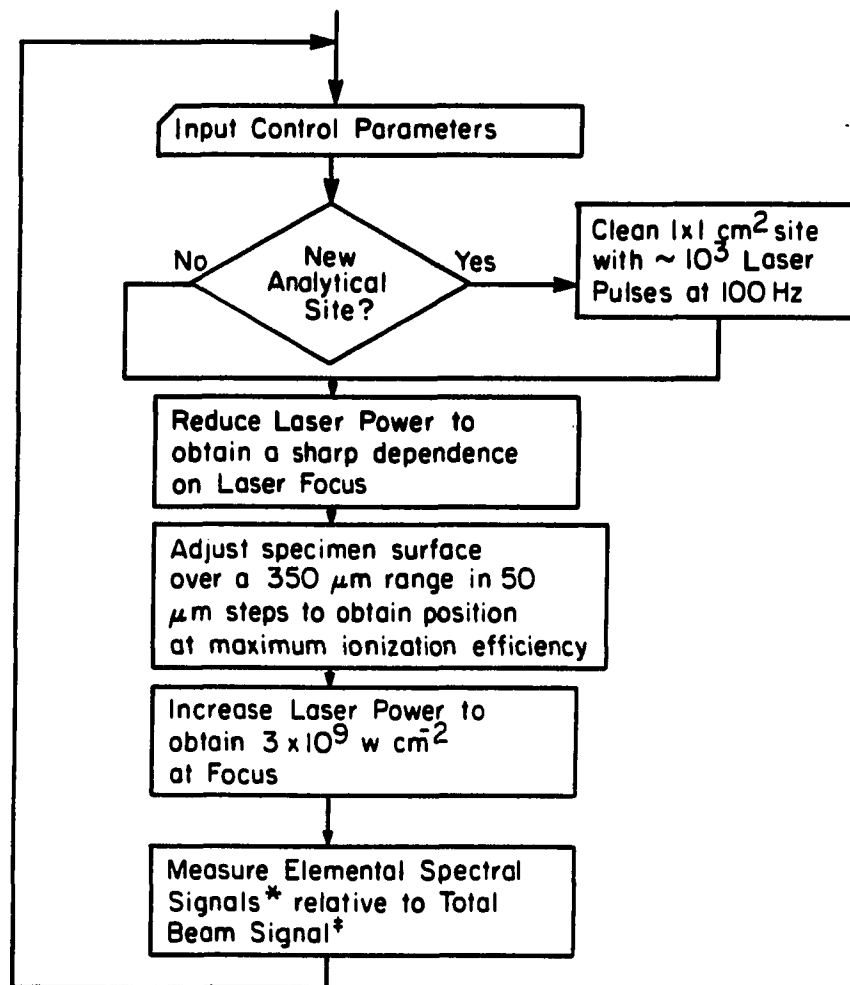


Figure 1. General computer algorithm for LMS control

metallic elements, Al and Ti, and two nonmetallic elements, P and S in NBS standard low alloy steel #466. Al and P were also determined in the NBS brass #C1100 in the same manner.

The results of the first experiment indicated that the highest power density available, $3 \times 10^9 \text{ W cm}^{-2}$, was the optimum setting. Using the highest power available the second experiment was conducted in which eight low alloy steel SRMs and three brass SRMs from the U.S. National Bureau of Standards were analyzed. The elements determined were selected because their concentrations were certified and their m/z values were within the switching range of the mass spectrometer. The major analyte isotope was monitored except in cases where a matrix ion peak interfered either by direct overlap (e.g, $^{58}\text{Fe}^+$ with $^{58}\text{Ni}^+$ in steel) or close proximity (e.g., $^{64}\text{Zn}^+$ with $^{63}\text{Cu}^+$ in brass). RSF data for each SRM were averaged over at least three complete measurement cycles (Fig. 1).

RESULTS AND DISCUSSION

Effects of Laser Power Density

The dependence of RSF values on laser power density is illustrated for representative elements in Fig. 2. The RSFs obtained for Al and Ti were at or above unity and were not greatly affected by laser power density. The RSF for Al in brass was apparently higher than that for Al in steel, although at $3 \times 10^9 \text{ W cm}^{-2}$ the observed difference was small relative to the uncertainty of the two measurements. The RSFs for P (ionization energy = 10.49 eV) and S (10.36 eV) were below unity but increased significantly as power density increased. The RSF for P in brass also merged closer to that for P in steel as power density increased. These results indicate that even higher power densities than those achievable with this laser are needed if uniform RSFs for elements of varying ionization energies in different sample matrices are desired (7). This conclusion also differs from that in our previous work in which the RSCs were essentially unity for C (11.26 eV), N (14.53 eV), and O (13.62 eV) in various metals despite the high ionization energies of these analyte elements. A higher laser power density of $5 \times 10^9 \text{ W cm}^{-2}$ was attained in this earlier study which probably accounts for this difference, i.e., the laser head is now less efficient and transmission of the optical components have degraded. It is also likely that the volatility of a given element and the strength with which it is bound to the sample matrix affect the RSC value in the power density range examined in this study.

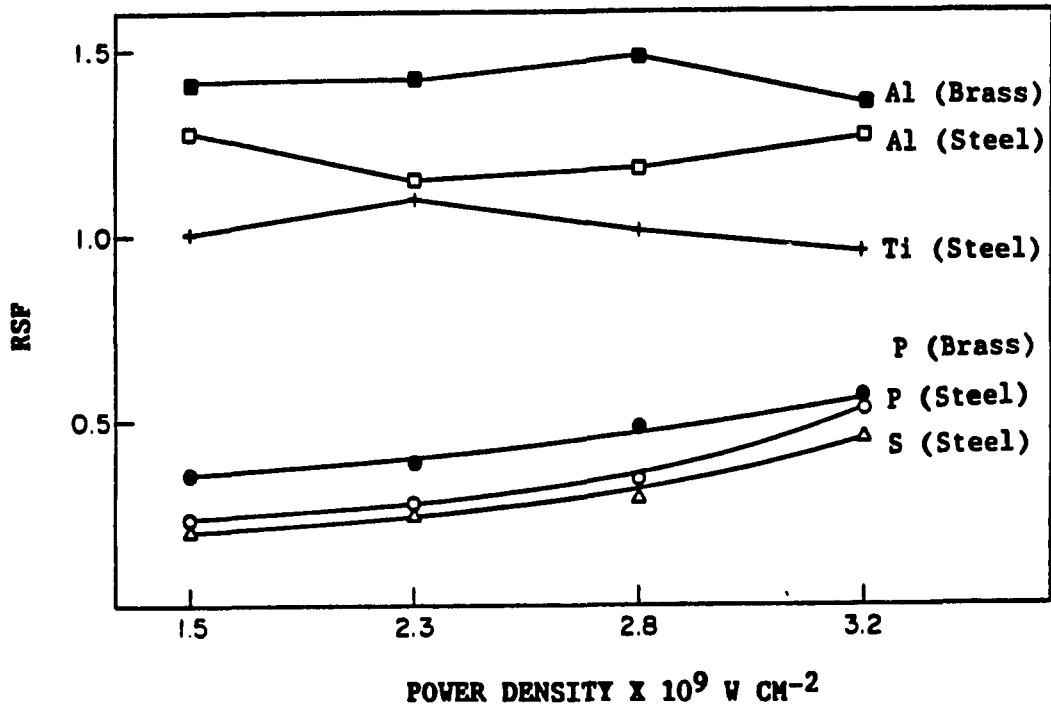


Figure 2. Plot of RSPs vs. laser density

Analytical Results for Steels and Brasses

The resulting RSF values obtained from analysis at the highest power density available are listed in Tables II and III from which the following observations were made. First, the RSF for Mn in steel was consistently high. The $^{55}\text{Mn}^+$ peak was adjacent to the massive $^{54}\text{Fe}^+$ and $^{56}\text{Fe}^+$ peaks, which likely caused a positive bias in the determination of Mn. A similar interference probably caused the high RSF for Zn in brass. For ionization of brass, the matrix peaks (Cu^+ and Zn^+) were considerably removed from Mn^+ , and here the RSF for Mn was essentially unity. Second, the RSFs decline steadily as the mass of the analyte increased. The ionization energies of the elements studied also decrease in this order, and the transmission of the mass spectrometer and/or the efficiency of the detector may have been m/z -dependent as well. Third, the RSFs were more uniform for analysis of brass than for steel. Nevertheless, assumption of uniform ionization efficiency yielded reasonable semiquantitative accuracy (i.e., $\pm 50\%$ relative or better as indicated by the deviations of RSF from unity) for the elements and sample types studied.

The median value of relative deviation for the results in Tables 2 and 3 was 6%. RSF values are not listed in Table 2 for V and Cr in SRM 465 even though they were definitely detectable. These two elements are certified to be present at 20 and 40 parts-per-million-atomic (ppma) in these samples, and the poor precision with which the analyte ion current could be measured precluded meaningful determinations of RSFs in these cases. Detection limits were estimated to be in the 10 ppma range

Table 2. RSF values for elements in steels

SRM #461	#462		#463		#464		#465			
Conc. Wt.%	RSF (%Rel. dev.)	Conc. Wt.%	RSF (%Rel. dev.)	Conc. Wt.%	RSF (%Rel. dev.)	Conc. Wt.%	RSF (%Rel. dev.)	Conc. Wt.%	RSF (%Rel. dev.)	
V	0.024	0.98 (4.2)	0.058	1.22 (9.1)	0.10	1.43 (5.1)	0.029	1.38 (9.4)	0.002	---
Cr	0.13	1.02 (1.5)	0.74	1.12 (6.1)	0.26	1.45 (4.0)	0.078	1.08 (11.3)	0.004	---
Mn	0.35	1.24 (5.2)	0.94	1.22 (5.7)		1.43 (5.3)	1.15	1.30 (14.3)	0.032	1.45 (11.6)
Fe	---	1.0 ^a (2.6)	---	1.0 (4.2)	---	1.0 (6.2)	---	1.0 (4.3)	---	1.0 (3.5)
Co	0.26	0.84 (3.3)	0.11	0.92 (7.9)	0.013	0.71 (4.0)	0.028	0.82 (2.1)	0.008	0.80 (14.5)
Ni	1.73	0.71 (5.2)	0.70	0.92 (7.5)	0.39	0.72 (3.1)	0.135	0.61 (7.1)	0.026	0.65 (15.8)
Cu	0.34	0.61 (13)	0.20	0.82 (6.8)	0.47	0.75 (2.4)	0.094	0.52 (10.9)	0.019	0.52 (10.3)

^aAssumed from Equation (1).

#466		#467		#468		AVG RSF	SD	RSD(%)
Conc. Wt.% dev.)	RSF (%Rel. dev.)	Conc. Wt.% dev.)	RSF (%Rel. dev.)	Conc. Wt.% dev.)	RSF (%Rel. dev.)			
0.007	1.01 (1.0)	0.041	1.28 (3.2)	0.17	1.56 (11)	1.27	0.21	16
0.011	0.98 (1.0)	0.036	1.07 (3.8)	0.54	1.54 (7.8)	1.18	0.15	12
0.11	1.12 (1.2)	0.27	1.40 (4.4)	0.47	1.42 (5.8)	1.32	0.12	9.2
---	1.0 (6.2)	---	1.0 (4.4)	---	1.0 (4.1)	1.0	---	---
0.046	0.85 (2.7)	0.074	0.84 (6.2)	0.16	0.85 (6.1)	0.83	0.059	7.1
0.051	0.77 (6.7)	0.088	0.64 (11.1)	1.03	0.71 (6.20)	0.72	0.098	14
0.033	0.66 (6.1)	0.067	0.57 (6.7)	0.26	0.65 (6.1)	0.64	0.10	16

Table 3. RSF Values for Elements in Brasses

	SRM C1100		C1101		C1102		AVG RSF	SD	RSD(%)
	Conc. Wt.%	RSF (%Rel. dev.)	Conc. Wt.%	RSF (%Rel. dev.)	Conc. Wt.%	RSF (%Rel. dev.)			
Mn	0.003	1.11 (10)	0.005	1.05 (1.5)	0.004	0.99 (1.6)	1.05	0.05	4.8
Fe	0.072	1.00 (6.6)	0.037	1.00 (1.6)	0.011	1.00 (7.4)	1.00	---	---
Ni	0.052	0.85 (4.9)	0.013	0.98 (11)	0.005	1.07 (0.22)	0.97	0.11	11
Cu	67.43	0.86 (5.3)	69.50	0.91 (0.16)	72.85	0.90 (2.4)	0.89	0.11	13
Zn	32.20	1.23 (15)	30.34	1.16 (2.0)	27.10	1.54 (6.1)	1.31	0.23	18
As	0.019	0.46 (1.8)	0.009	0.42 (11)	0.004	0.55 (10)	0.48	0.07	14

for the elements shown in Tables 2 and 3. The ionization and detection efficiency for various elements is more nearly uniform for this LMS instrument than for the laser microprobe mass analyzer (LAMMA), the latter of which is generally used for qualitative characterization rather than quantitative elemental analysis (e.g., 26 articles describing this instrument and its application in *Fresenius Z. Anal. Chem.*, 308 (1981) 193-320). The ionization efficiency is also more nearly uniform for this LMS device than for spark source MS (8), glow discharge MS (9), or secondary ion MS (10). Extrapolation of Figure 2 and earlier studies (11) indicates that use of a laser with only slightly higher power density ($\sim 5 \times 10^9 \text{ W cm}^{-2}$) could further improve the uniformity of ionization efficiency, particularly for nonmetallic and metalloid elements.

Determination of Oxygen in Silicon

Figure 3 gives the calibration curve for the determination of oxygen in silicon. The curve is linear up to ~5% atomic and the detection limit is approximately 10 ppma. A precision of 10% relative standard deviation can be achieved when the system has been carefully optimized by monitoring the Si^{+2} signal, which is sensitive to laser power fluctuations (5).

Compared with other analytical techniques, analysis of the standards using fast neutron activation yielded poor accuracy and reproducibility due to the limited sample size. Vacuum fusion gas analysis and inert gas fusion have traditionally been used for this type of analysis, but extension of these techniques to the analysis of

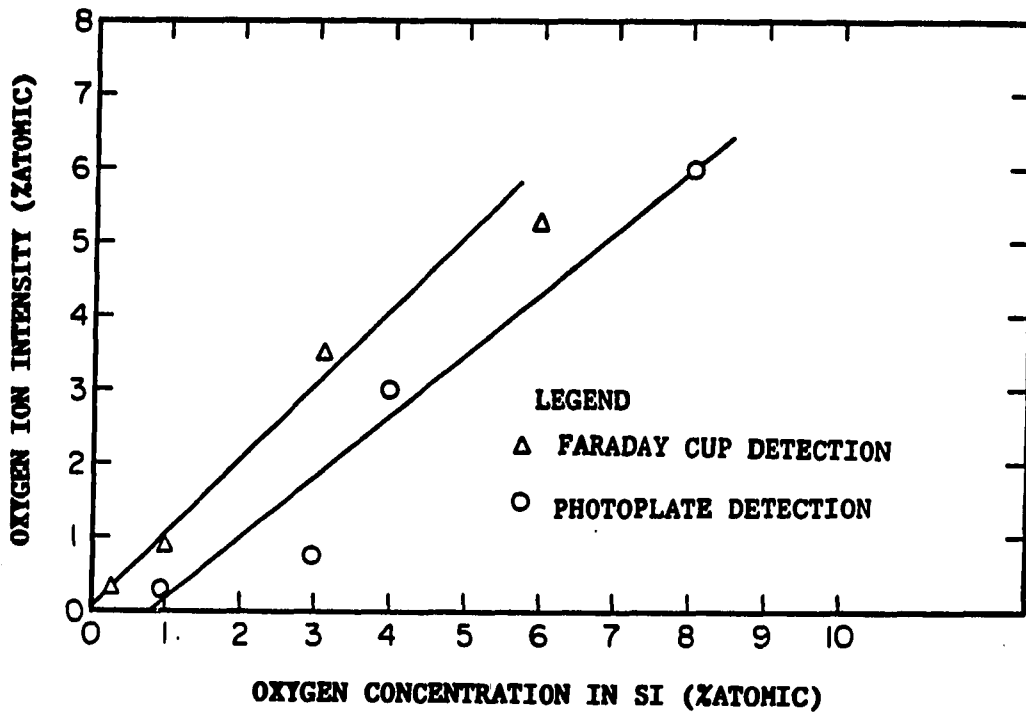


Figure 3. Oxygen ion intensity vs. Oxygen concentration in Si

silicon would require extensive optimization studies. Infrared (IR) spectroscopy is one of the standard techniques to determine the oxygen in silicon by measuring the Si-O-Si vibration at 9 μm due to interstitial oxygen (12). However, interference owing to the high absorption from matrices and insensitivity to non-interstitial oxygen (13) limit the IR technique especially for high oxygen levels. Other instrumental methods such as secondary ion mass spectrometry (SIMS) are also widely used to measure total oxygen content in heavily doped silicon materials. The SIMS technique is limited for quantitation because of high oxygen backgrounds and it is well known that secondary ion yields vary quite drastically for different elements and for the same element in different matrices (14). There still is no standard reference material certified for oxygen in silicon, largely because of the shortcomings of these techniques. Thus LMS appears to be a promising development for determining trace level or macro amounts of oxygen in silicon or in other semiconductors, although further studies are needed.

CONCLUSION

The observations reported indicate that LMS may ultimately achieve quantitative determination of elements in solids without standards (8). We are in the process of altering our experimental arrangement to permit operation at higher ion accelerating voltages, with a smaller laser spot size (by a factor of 2), and with a higher power laser. The Faraday cup detector used here restricts detection limits to approximately 10 ppma due to its inherent zero amplification and to background fluctuations caused by secondary electron emission. These detection limits could doubtless be improved and the secondary electron problem eliminated by substituting an electron multiplier or a Daly detector. The analytical capabilities of LMS for non-conducting samples will also be investigated.

LITERATURE CITED

1. Conzemius, R. J.; Capellen, J. M. Int. J. Mass Spectrom. Ion Phys. 1980, 34, 197.
2. Conzemius, R. J.; Junk, G. A. DOE/NBM-7001005, 1986.
3. Zhao Shankai; Conzemius, R. J.; Svec, H. J. Anal. Chem. 1984, 56, 382.
4. Conzemius, R. J.; Schmidt, F. A.; Svec, H. J. Anal. Chem. 1981, 53, 1899.
5. Conzemius, R. J.; Zhao Shankai; Houk, R. S.; Svec, H. J. Int. J. Mass Spectrom. Ion Processes 1984, 61, 277.
6. Conzemius, R. J. Ames Laboratory, Private Communication, 1987.
7. Ramendik, G. I.; Kryuchkova, O. I.; Ku-viladze, M. S.; Mchedlidze, T. R.; Tyurin, D. A. Zhurnal Analiticheskoi Khimii 1983, 38, 1749.
8. Bykovskii, Yu. A.; Basova, T. A.; Belousov, V. I.; Gladskoi, V. M.; Gorshkov, V. V.; Degtyarev, V. G.; Laptev, I. D.; Nevoilin, V. N. Sov. Phys. Tech. Phys. 1976, 21, 761.
9. Harrison, W. W.; Hess, K. R.; Marcus, R. K.; King, F. L. Anal. Chem. 1986, 58, 341A.
10. Tong, H. Y.; Karasek, F. W. Anal. Chem. 1984, 56, 2129.
11. Bykovskii, Yu. A.; Zhuravlev, G. I.; Belousov, V. I.; Gladskoi, V. M.; Degtyarev, V. G.; Kolosov, Yu. N.; Nevolin, V. N. Sov. J. Plasma Phys. 1978, 4, 180.
12. Kaiser, W.; Kech, P. H.; Lang, C. F. Phys. Rev. 1956, 101, 1262.

13. Chu, P. K.; Hockett, R. S.; Wilson, R. G. Mat. Res. Soc. Symp. Proc. 1986, 59, 67.
14. Storms, H. A.; Brown, K. F.; Stein, J. D. Anal. Chem. 1977, 49, 2023.

**SECTION V. SCINTILLATION-TYPE ION
DETECTION FOR INDUCTIVELY COUPLED PLASMA MASS SPECTROMETRY**

SCINTILLATION-TYPE ION DETECTION FOR INDUCTIVELY
COUPLED PLASMA MASS SPECTROMETRY

L. Q. HUANG, S. J. JIANG AND R. S. HOUK

AMES LABORATORY-USDOE AND DEPARTMENT OF CHEMISTRY

IOWA STATE UNIVERSITY

INTRODUCTION

Inductively coupled plasma mass spectrometry (ICP-MS) has become an important new technique for elemental and isotopic analysis (1-3). In all the ICP-MS instruments constructed to date, the ion signals are monitored by an electron multiplier, which is generally of the Channeltron variety (4). Although good analytical performance can certainly be obtained with Channeltron electron multipliers, they do have several undesirable characteristics as detectors for ICP-MS. A Channeltron has a limited lifetime of approximately 1 year under normal analytical use. The general use of pulse counting techniques, in which a high bias voltage is applied to the multiplier so that its gain is saturated, probably accelerates the rate of gain loss. The response of a Channeltron is linear up to count rates of approximately 1×10^6 counts s^{-1} ; above this value, calibration curves tend to droop. Deviation from linear response at high count rates particularly limits the concentration range over which either very large or very small isotope ratios may be determined (5) and can be a source of error when isotope dilution is employed for quantitation (6). Conceivably, the linear range could be improved by employing a segmented Channeltron that permits both analog current measurements and pulse counting at the same time. There is some evidence that the detector gain can be degraded temporarily by scanning the mass analyzer across an intense peak, e.g., $> 10^7$ counts s^{-1} . If a peak for a trace analyte is monitored soon after the intense peak, this "fatigue" can affect the accuracy with which the trace constituent may be determined or limit the rate at which the

spectrum can be scanned (7). Although computer-controlled peak hopping routines can be devised to avoid exposing the detector to the intense ion beam, this often requires prior knowledge of the major element composition of the sample and can be inconvenient.

The scintillation device depicted by items J-L in Figure 1 is an alternation ion detector for mass spectrometry. Its operation is based upon the following sequence of events. Ions from the mass analyzer (G) strike the negative target (J) and generate secondary electrons. These electrons are accelerated from the target (~ -5 kV) to a thin grounded metal film coated on the surface of a scintillator (K). The film thickness is chosen so that the secondary electrons can penetrate the film and deposit energy in the scintillator. Energy deposition promotes some of the scintillator molecules to excited electronic states. The excited molecules then emit photons at visible wavelengths that are sensed by the photomultiplier (L). This technique is often referred to as Daly detection after its inventor (8-10). A scintillation-type detector offers some potential advantages in the problem areas identified above for Channeltron electron multipliers. At the very least, the gain of the scintillation detector should not deteriorate with time. In the present work, the analytical figures of merit of a scintillation-type detector are compared with those of a Channeltron for ICP-MS.

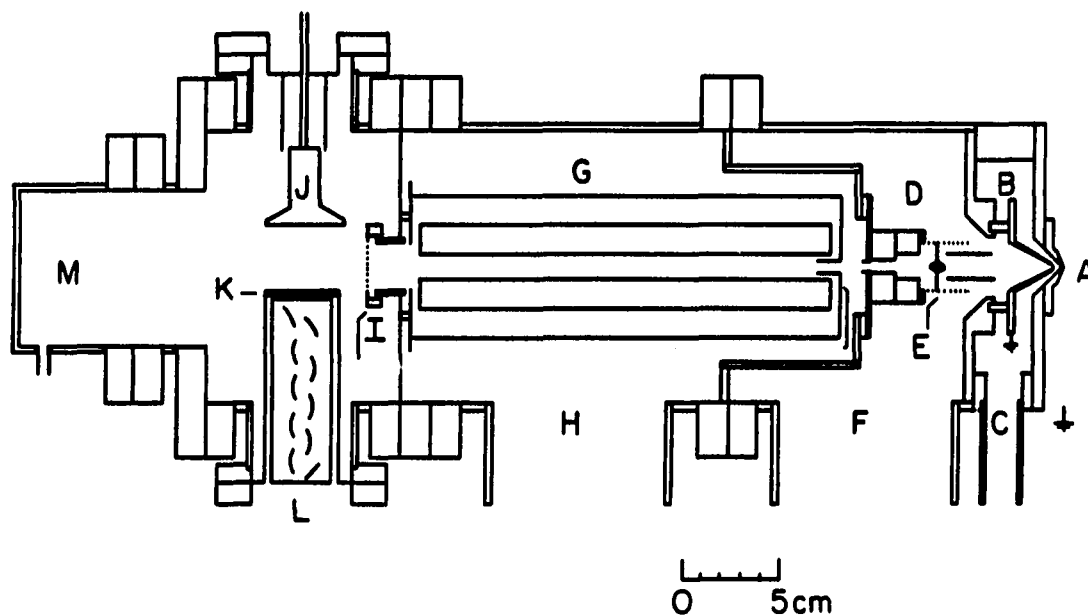


Figure 1. Schematic diagram of MS (ICP not shown): A - sampler, B - skimmer, C - port to rotary pump, D - ion lens (voltage settings listed), E - photon baffle, F - port to diffusion pump (1600 L s^{-1}), G - quadrupole mass analyzer, H - port to diffusion pump (800 L s^{-1}), I - exit lens (voltage settings listed), J - Al target (-5 kV), K - Al coated scintillator, L - PHT, M - turbomolecular pump (150 L s^{-1})

EXPERIMENTAL

The sampling interface and MS part of the apparatus are depicted in Figure 1. Instrumental components and operation conditions are identified in Table 1.

ICP-MS Apparatus

The basic features of the ultrasonic nebulizer, ICP, sampling interface, ion optics, mass filter, and vacuum system have been described previously; pertinent alterations are noted below. The load coil was grounded at its downstream end to the shielding box as shown in Figure 2Y of Reference 15. The maximum ion kinetic energy was lower (i.e., approximately +10 V) and less strongly dependent on aerosol gas flow rate than was the case in Reference 16, indicating that the residual discharge was less severe in the present work. A photon stop consisting of two metal cones (E, Figure 1) was added to the ion lens. These cones were kept at the same potential. Ions leaving the mass analyzer went through a stainless steel cylinder (2.5 cm long x 1.8 cm inside diam.) with a wire grid at its downstream end. Separate potentials were applied to these ion optical elements to transmit ions into the detector. This assembly also served as the differential pumping orifice between the quadrupole and detector chambers.

Table 1. Instrumental Facilities

Component	Operating conditions, materials, or dimensions
Nebulization: Continuous flow ultrasonic nebulizer (11)	Desolvation temperature 80 C Solution uptake rate 2.5 mL min ⁻¹
ICP generator and torch (12)	Operating conditions described in Ref. (13)
Ion extraction interface: Ames Laboratory construction (14)	Sampling position on center 10 mm from load coil. Sampling orifice 0.7 mm diam. Skimmer orifice 1.2 mm diam. Sampler-skimmer separation 8 mm.
Turbomolecular pump on detector chamber: Model TMP/NT 150 Leybold-Heraeus	Operating pressures (see Figure 1) expansion chamber 1 torr second chamber ~ 1 x 10 ⁻⁴ torr quadrupole chamber 2 x 10 ⁻⁶ torr detector chamber 1 x 10 ⁻⁶ torr
Mass analyzer: Model 270-9 with O12-15 RF head Extranuclear Laboratories (now Extrel)	Mean rod bias -1 V DC.
Scintillator: Model NE104 EMI	
PMT: Model 9924B EMI	PMT bias voltage - 800 V. Target bias voltage - 5000 V. Output pulse width 30 ns (FWHM)
Counting electronics: Model 1763 preamplifier Model 1762 amplifier-discriminator Photochemical Research Associates	Maximum count rate capability 20 MHz. Pulse width 40 ns TTL output
Data acquisition Model 1170 signal averager Nicolet, Inc.	Maximum count rate capability 20 MHz
LSI 11/23 - based minicomputer Digital Equipment Corp.	Software and interfaces produced at Ames laboratory (14).

Scintillation Detector

The aluminum target was polished to a mirror finish. A power supply with a very high maximum voltage output (30 kV) was used to bias the target as suggested by previous studies with this detector (8). However, in the present work the background and background noise increased considerably as the magnitude of the target bias increased; the signal-to-noise ratio was optimum at the relatively low target voltage shown in Table 1. It is interesting to note that this optimum target bias (~ -5 kV) was similar to the optimum voltage found for deflecting ions into a Channeltron (14).

The scintillator was coated with Al by glow discharge sputtering and vapor deposition. The Al layer was approximately 20 nm thick and was grounded to the vacuum chamber. A scintillator material with a short decay time (2 ns) and an inexpensive PMT with a reasonably small pulse width (30 ns FWHM) were selected to minimize counting losses at high count rates. The photomultiplier was kept in its own glass enclosure, i.e., it was not evacuated by the pump on the detector chamber. The RF leads to the mass filter did not pass through the detector chamber so that RF interference from the quadrupole power supply was not encountered. Other electrical leads and connections were also kept out of the detector chamber to prevent formation of an electrical discharge therein. The detector chamber was evacuated by a separate turbomolecular pump and was maintained at a slightly lower pressure than the chamber housing the mass analyzer (Table 1). Ideally, the pressure in the detector chamber should be as low as possible because the

background decreases and a higher target bias can be tolerated at lower pressure.

Data Acquisition

Data were obtained in three modes. Stability was evaluated by selected ion monitoring, i.e., the mass analyzer transmitted only the m/z value of interest for the entire measurement cycle. Calibration curves and isotope ratios were determined in the multichannel scanning mode using the signal averager. The m/z range was restricted such that the full 4096 memory addresses spanned only the isotopes of interest. The dwell time was $100 \mu\text{s address}^{-1}$ and 256 sweeps were averaged; this process took 105 s for each element. The individual peaks in the averaged spectra were integrated by summing the total counts in the range of memory addresses corresponding to each peak (3,5). The background was determined in each m/z interval of interest by analysis of an appropriate blank solution. The background was then subtracted from the gross integrated signal before the isotope ratio was calculated. Detection limits were determined by adding 10 scans across each major isotope in 10 s each scan. The peak height for each element was measured from this averaged spectrum, and the background level and standard deviation were determined by analyzing a blank solution and averaging the counts in adjacent m/z addresses spanning the center of each analyte peak. The detection limit represented the solution concentration necessary to yield a net peak height equivalent to three times the standard deviation of the background.

Solutions and Standards

The solvent was 1% HNO_3 in distilled deionized H_2O . Standard solutions were 1 mg L^{-1} of each element unless noted otherwise and were prepared by dilution aliquots of commercial stock solutions (Fisher).

RESULTS AND DISCUSSION

General Observations

One reason for evaluating the scintillation detector was the expectation that it would not respond at all to photons from the ICP. Therefore, we thought the detector could be positioned directly behind the exit lens of the mass analyzer, and no optical baffle would be necessary in the ion lens. This optical baffle is definitely a source of ion loss (14, 17) and possibly is also a cause of m/z discrimination. However, the background was high and erratic without a photon baffle, so one was inserted into the ion lens (Figure 1). With the photon baffle present, the background was typically 500 ± 25 counts s^{-1} using the scintillator detector. This latter level of background and standard deviation were similar to those obtained in earlier studies with a Channeltron detector with the photon baffle present. Possible reasons for the high background with the photon stop absent included ionization of excited neutral species (e.g., metastable Ar atoms) under the influence of the target voltage, a discharge caused by a high local density of species in the supersonic beam travelling between the target and the PMT, or emission of photoelectrons from bombardment of the target by plasma photons, particularly those in the vacuum ultraviolet region (18, 19).

Precision of Isotope Ratio Measurements

Isotope ratios were determined repetitively for several elements. The results are listed in Table 2. The primary figure of merit in isotope ratio measurements is precision. With the scintillation detector the precision for each isotope ratio was better by a factor of two than that typically obtained with this ICP-MS device using a Channeltron detector. For example, in previous work with a Channeltron, isotope ratios near unity (i.e., in the range 0.5 to 3) could be determined with a relative standard deviation of 1 to 2 % (14, 20, 21) compared to 0.3 to 1 % using the scintillation detector (Table 2) for ion count rates and data acquisition times that were comparable for the two detectors. The precision obtained with the scintillator was either comparable to that expected from counting statistics or was worse than the counting statistics limit by up to a factor of two (e.g., Rb and Dy in Table 2). For comparable measurement times (~ 100 s) with Channeltron detectors, the precision for isotope ratio measurements was generally worse than the counting statistics limit by a larger factor (typically two or three) (22). Thus, at least for this ICP-MS device, the scintillator detector offered significant improvement in precision for isotope ratio determinations. Comparison of the determined ratios with the expected natural abundance ratios indicated some bias; the extent of bias was similar to that seen with a Channeltron and was probably due to mass discrimination by the mass filter. The magnitude of the bias was not consistent from element to element in Table 2

Table 2. Isotope Ratio Determinations

Element	Concentration (mg L ⁻¹)	Isotope Ratios		Rel. St'd Deviations(%)		
		Isotopes	det'd.	nat'l.	det'd ^a	counting statistics
Cu	1	63/65	2.15	2.24	0.4	0.37
Zn	3	64/66	1.73	1.76	0.7	0.64
		64/67	9.76	11.9	3.2	1.81
		64/68	2.59	2.63	0.8	0.79
Rb	1	85/87	2.45	2.60	0.4	0.2
Ce	1	140/142	7.66	7.97	0.5	0.56
Dy	2	160/162	0.0973	0.0899	0.9	1.94
		161/162	0.734	0.74	0.9	0.48
		163/162	0.996	0.987	0.8	0.43
		164/162	1.13	1.10	0.7	0.41
Tl	1	205/203	2.44	2.39	0.3	0.29

^aDetermined from 7-8 separate measurements of each isotope ratio.

because the resolution of the mass spectrometer was optimized separately for each element to minimize bias and to provide proper peak shapes.

Detector "Fatigue"

The following experiment was performed to determine whether the scintillator detector suffered any gain loss while scanning over an intense peak. The mass analyzer was scanned in the range $m/z = 154 - 161$. Gadolinium isotope ratios ($m/z = 155, 156, \text{ and } 160$) were measured for a sample solution containing only Gd; these data are shown in the first row of Table 3. Next, Gd isotope ratios were determined for a solution containing the same Gd concentration but with Tb present at 15 mg L^{-1} . Thus, the detector sensed the massive ^{159}Tb peak ($\sim 1 \times 10^7$ counts s^{-1}) immediately before the ^{160}Gd peak on each scan. As shown in the second row of Table 3, the Gd isotope ratios were unaffected by the presence of Tb. The Gd isotope ratio was also independent of the sweep rate even at the fastest rate used ($5 \text{ } \mu\text{s address}^{-1}$, $20 \text{ ms per full sweep}$), which was the fastest the mass analyzer could be swept with adequate resolution between Tb and Gd peaks. This indicated that the scintillation detector did not lose gain by scanning across the large ^{159}Tb peak. The precision of the Gd isotope ratios was similar in the presence or absence of Tb. In this experiment, the resolution of the mass analyzer had to be increased (relative to that used for the isotope ratios in Table 2) to properly separate the Gd and Tb peaks. Operation at higher resolution yielded a) lower ion count rates, b) more sharply pointed peaks that were less reproducible from scan to scan, and c)

Table 3. Ratio Measurements for Selected Gd Isotopes

Solution	¹⁵⁵ / ₁₆₀			Gd Isotope Ratios for m/z = ¹⁵⁶ / ₁₆₀		
	nat'l.	det'd.	RSD ^a (%)	nat'l.	det'd.	RSD ^a
1 mg L ⁻¹ Gd	0.673	0.836	2.3	0.934	1.07	1.6
1 mg L ⁻¹ Gd + 15 mg L ⁻¹ Tb	0.673	0.834	1.7	0.934	1.06	1.2

^aRelative standard deviation of 5-6 determinations.

more extensive discrimination against ions at higher m/z . For these reasons, the accuracy and precision of the Gd isotope ratios were poorer than those for other elements with comparable ratios (e.g., Zn and Dy) in Table 2. Because the point of this experiment was to look for gain loss, no particular effort was expended to minimize the bias or optimize the precision of the determined isotope ratios.

The resistance of the scintillation detector to long-term gain degradation was illustrated by the following observations. As a first step toward optimization, the plasma conditions, sampling position, ion lens voltages, etc., were adjusted to yield maximum signals for the major background ions (e.g., O^+ , H_2O^+ , Ar^+ , and ArH^+). In this mode, the ion current was detected by analog means and the spectrum was displayed continuously on an oscilloscope. With a Channeltron, permanent gain loss occurred in 10 hours or less unless the detector bias voltage was lowered from approximately -3 kV (i.e., a value useful for pulse counting) to -2.2 - -2.5 kV. In contrast, no loss of gain was apparent with the scintillator if the major ions were monitored at the same target voltage and PMT bias voltage as would be used for pulse counting detection. It is clear that the scintillation detector is more resistant to gain degradation than the Channeltron, although there may well be limits to the former's tolerance to intense ion beams not elucidated by the present work.

Linear Dynamic Range and Stability

A typical calibration curve obtained with the scintillation detector is shown in Figure 2. The curve was linear (correlation coefficient = 0.9998) up to a Tb concentration that yielded 2×10^6 counts s^{-1} . With the same counting electronics, calibration curves obtained with a Channeltron begin to droop below the straight line at lower count rates (typically 1×10^6 counts s^{-1}) (22,23). Thus, the linear responses for the scintillation detector extended to somewhat higher count rates than for a Channeltron.

At higher count rates, the experimental curve (solid line, Figure 2) was below the linear extrapolation because of counting losses. For example, at 3×10^6 counts s^{-1} , the experimental count rate was below the straight line by approximately 12 %. This extent of counting loss corresponded to an overall dead time of $(0.12)/(3 \times 10^6) \approx 40$ ns (24), which agreed with the specifications for the PMT and counting electronics (Table 1). Use of counting electronics and PMTs with still faster response times could further extend the linear range accessible with a scintillation detector.

To evaluate the stability obtainable with the scintillation detector, the count rate at $m/z = 140$ for a 0.5 mg L^{-1} solution of Ce was measured every 2 s for two hours. The relative standard deviation of these 3600 measurements was 5%. The average count rate for 5 adjacent measurements at the end of the two hour period differed from that at the beginning of the period by only -5% relative, i.e., the

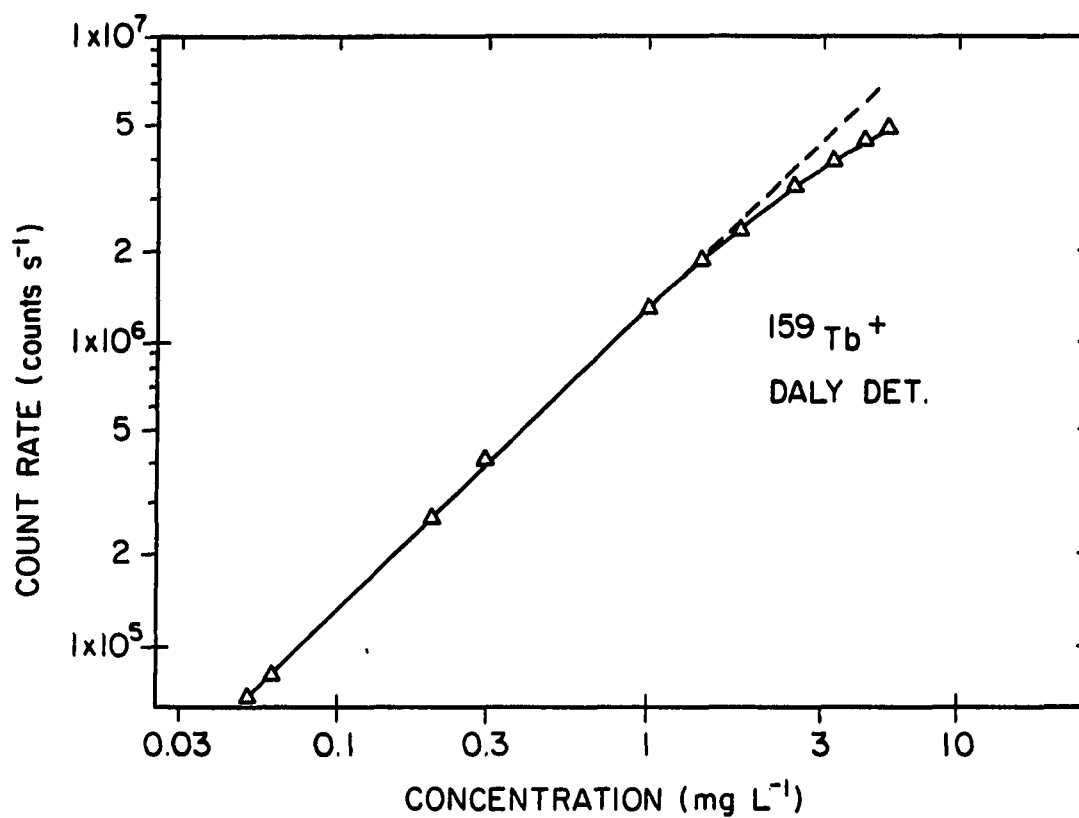


Figure 2. Calibration curve for $^{159}\text{Tb}^+$ (The dotted line represents the extrapolation of the linear section.)

sensitivity did not drift greatly over the two hour period. With Channeltron detection, the sensitivity generally drifted by $\pm 10\%$ over one hour with a relative standard deviation of 10%. With the scintillation detector, the figures of merit for stability were considerably better than we have achieved with Channeltron detection for this particular ICP-MS device; they also rival the stability performance of the present commercial instruments (25). The 5% relative standard deviation was still much worse than that expected from counting statistics alone (approximately 0.3% at these count rates). The stability performance of an ICP-MS device doubtless arises from the juxtaposition of various factors such as nebulizer fluctuations, deposition of material on the sampling interface and ion optics, and variability of the resolution and transmission characteristics of the mass analyzer with time. The present work indicates that the detector may contribute to drift and instability as well.

Detection Limits and Sensitivities

These figures of merit are listed in Table 4. The sensitivities and detection limits obtained with the scintillation detector are similar to those obtained with this ICP-MS device with a Channeltron detector and with the photon stop (Figure 1) present. Naturally, the sensitivities described in Table 4 are poorer (by factors of 5-10) than those obtained previously without a photon stop in this instrument (14,17). Furthermore, the sensitivities in Table 4 are comparable to those

Table 4. Detection Limits (3σ) and Sensitivities

Element	Ionization Energy (eV)	Sensitivity (counts s^{-1} per mg L^{-1})		
		actual	norm. to isotopic abundance	Detection Limit ($\mu g L^{-1}$) ^a
⁵² Cr	6.77	147,000	175,000	1
⁵⁹ Co	7.86	170,000	170,000	0.9
⁶³ Cu	7.73	71,000	103,000	2
⁶⁴ Zn	9.39	26,000	53,000	6
⁷⁵ As	9.81	28,000	28,000	5
⁸⁵ Rb	4.18	124,000	172,000	1
⁸⁸ Sr	5.70	153,000	185,000	1
⁸⁹ Y	6.38	240,000	240,000	0.6
⁹⁰ Zr	6.84	85,000	165,000	2
⁹³ Nb	6.88	113,000	113,000	1
⁹⁸ Mo	7.10	38,000	160,000	4
¹⁴⁰ Ce	5.47	234,000	264,000	0.6
¹⁴² Nd	5.49	64,000	236,000	2
¹⁵² Sm	5.63	82,000	308,000	2
¹⁵³ Eu	5.67	226,000	434,000	0.7
¹⁵⁹ Tb	5.85	401,000	401,000	0.4
¹⁶⁴ Dy	5.95	93,000	330,000	2
²⁰⁵ Tl	6.11	126,000	179,000	1
²⁰⁸ Pb	7.42	92,000	178,000	2

^aDetection limits quoted in terms of overall mass of element with mass analyzer monitoring isotope indicated.

obtained with the commercial instruments; detection limits are poorer in present work because the standard deviation of the background is higher. Although it was initially expected that the detection limits would be much better with the scintillation detector, this did not prove to be the case.

CONCLUSION

The performance of the scintillator detector is either comparable or superior to that of a Channeltron electron multiplier with the particular ICP-MS instrument used. The initial cost of the scintillator detector is higher than that of the channeltron, particularly if the scintillator requires an additional pump and vacuum chamber. However, the cost and inconvenience of replacing a dying Channeltron are not encountered with the scintillator, which compensates for the higher initial cost of the latter detector. Additional improvements in the performance of the scintillator could be possible by reduction of the background pressure or by offsetting both the target and PMT above or below the center line of the sampler, skimmer, and mass analyzer.

LITERATURE CITED

1. Douglas, D. J.; Houk, R. S. Prog. Anal. Atomic Spectrom. 1985, 8, 1.
2. Houk, R. S. Anal. Chem. 1986, 58, 97A.
3. Gray, A. L. Spectrochim. Acta 1985, 40B, 1525; 41B, 151.
4. Kurz, E. Am. Lab. 1979, 11, 67.
5. Chong, N. S.; Houk, R. S. Appl. Spectrosc. 1986, 41, 66.
6. Paulsen, P. Pittsburgh conference, Anal. Chem. Appl. Spectrosc., Atlantic City, March, 1986; Paper No. 3.
7. Brown, R. Elemental Research Inc., North Vancouver, B. C. Canada, personal communication, 1985.
8. Daly, N. R. Rev. Sci. Instrum. 1960, 31, 264.
9. Gibbs, H. M.; Commins, E. D. Rev. Sci. Instrum. 1966, 37, 1385.
10. Ridley, B. W. Nucl. Instrum. Meth. 1961, 14, 231.
11. Bear, B. R.; Fassel, V. A. Spectrochim. Acta 1986, 41B, 1089.
12. Scott, R. H.; Fassel, V. A.; Kniseley, R. N.; Nixon, D. E. Anal. Chem. 1974, 46, 75.
13. Jiang, S. J.; Houk, R. S. Anal. Chem. 1986, 58, 1739.
14. Olivares, J. A.; Houk, R. S. Anal. Chem. 1985, 57, 2674.
15. Gray, A. L.; Houk, R. S.; Williams, J. G. J. Anal. Atomic Spectrom. 1987, 2, 13.
16. Olivares, J. A.; Houk, R. S. Appl. Spectrosc. 1985, 40, 1070.
17. Houk, R. S. "Analytical Chemistry in the Exploration, Mining and Processing of materials", Butler, L. R. P., Ed.; Blackwell: Oxford, 1986; Chapter 3.

18. Houk, R. S.; Fassel, V. A.; LaFreniere, B. R. Appl. Spectrosc. 1986, 40, 94.
19. LaFreniere, B. R.; Houk, R. S.; Fassel, V. A. Anal. Chem. 1987, submitted.
20. Jiang, S. J.; Houk, R. S. Spectrochim. Acta 1987, 42B, 93.
21. Serfass, R. E.; Lindberg, G. L.; Olivares, J. A.; Houk, R. S. Proc. Soc. Biol. Medicine 1987, 186, 113.
22. Boorn, A. W.; Fulford, J.; Douglas, D. J., 1986 Winter Conference on Plasma Spectrochem., Kona, HI, Paper No. 15.
23. Tan S. H. Ph.D. Dissertation, University of Alberta, Edmonton, Alberta, 1987.
24. Skoog, D. A. "Principles of Instrumental Analysis", 3rd ed.; Saunders College Publishing: Philadelphia, 1985; P. 510.
25. Thompson, J. J.; Houk, R. S. Appl. Spectrosc. 1987, 41, 801.

SUMMARY AND FUTURE RESEARCH

This dissertation has primarily described preliminary results from the development of a new time-of-flight mass spectrometer.

We have demonstrated that high TOF mass resolution can be achieved when a short duration laser is combined with fast ion detection and data acquisition and that a sub-nanosecond pulsed laser can be used for "soft ionization" of large organic molecules. However, it would be a significant advance if the high mass resolution could be retained with thermally labile organic specimens. This advance will require more detailed studies of substrate preparation, specimen deposition, faster lasers, and a variety of different samples.

The study of ion association from individual TOF scans provides a new means of obtaining very useful information as described in Section II of this dissertation. This added parameter or resolution element should greatly increase the informing power of mass spectrometry. The associations should be better characterized when more control of ion current sources are realized. Applications of these associations should be expanded when organic and biochemical specimens are examined.

In future studies, installation of a ion reflector, addition of a neutral particle detector, and introduction of a pulsed Cs ion gun as shown in Figure 1 should greatly expand the power of the TOF-MS both in analytical applications and fundamental studies. Improved TOF-MS performance, particular in mass resolution, is expected because the ion reflector will compensate for peak broadening due to the ion energy spread, e.g., if the ions were monoenergetic and there were no

instrumental aberrations, the peak width would be 1 ns, the limit of accuracy of the TDC used. At 5 kV, an m/z 1000 ion takes $\sim 60 \mu\text{s}$ to make the 180 cm trip in the system. These figures correspond to a mass resolution of 60,000. The twin detector configuration plus the induced ion dissociation technique should provide "MS-MS" capability for organic structure elucidation as well as for metastable decay studies. The introduction of a pulsed Cs ion gun to TOF-MS should be useful for the study of secondary ion mass spectrometry (SIMS) in characterizing surfaces and as a complementary ionization technique for various solid specimens. The Cs ion gun will be very beneficial for the study of ion association since the primary ion beam of the gun can be easily manipulated so that the secondary ion current can be better controlled. Furthermore, the high repetition rate available with the gun (4 kHz, i.e., 4000 spectra sec^{-1}) will generate much more data in a short time allowing more reliable statistics in the study of ion association.

Finally, let me close this dissertation with a quotation from an old Chinese philosopher, Lao Tzu, that "If the greatest achievement is incomplete, then its usefulness is unimpaired" (see Figure 2).

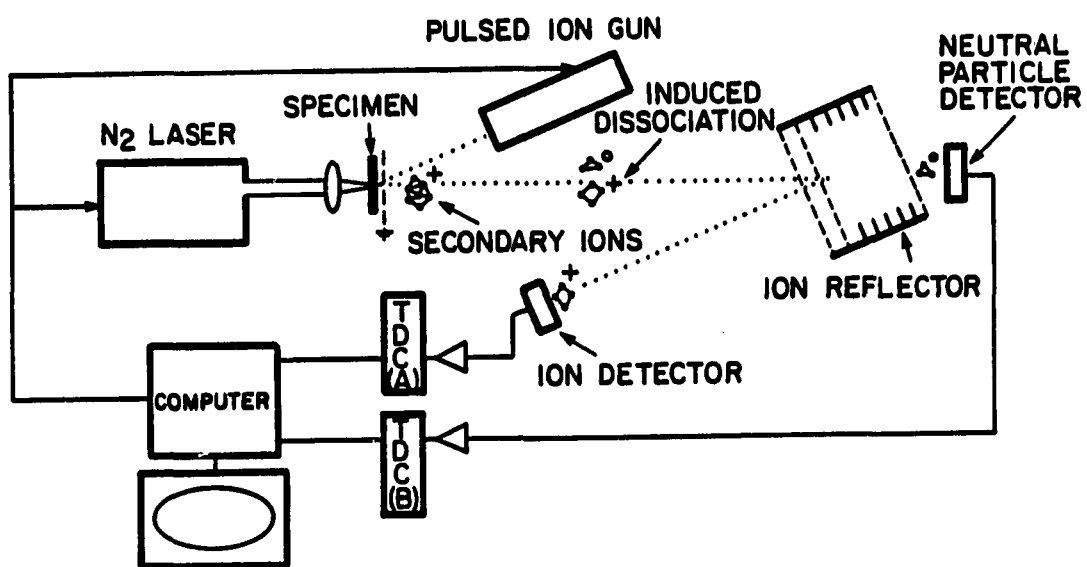



Figure 1. Schematic diagram of future TOF-MS



LAO TZU (500 B.C.)
FROM TAO TE CHING (# 45):

大成若缺・其用不弊・

**If the greatest achievement is incomplete,
Then its usefulness is unimpaired.**

Figure 2. Lao Tzu, First sentence of the 45th poem in Tao Te Ching

APPENDIX A

The χ^2 (chi-squared) distribution

ν^a	Confidence Level				
	97.5	99.0	99.5	99.9	99.95
1	5.024	6.635	7.879	10.83	12.12
2	7.378	9.210	10.60	13.82	15.20
3	9.348	11.34	12.84	16.27	17.73
4	11.14	13.28	14.86	18.47	20.00
5	12.83	15.09	16.75	20.52	22.11

^a ν = Degrees of freedom (i.e., $\nu = 1$ for TOF-MS).

APPENDIX B

Critical Values of the Correlation Coefficient, r_0

n ^a	Confidence Level					
	80%	90%	95%	98%	99%	99.8%
100	0.129	0.165	0.197	0.232	0.265	0.305
110	0.123	0.158	0.187	0.222	0.245	0.292
120	0.118	0.151	0.179	0.212	0.234	0.279
130	0.113	0.145	0.172	0.204	0.225	0.269
140	0.109	0.140	0.166	0.196	0.217	0.259
150	0.105	0.135	0.160	0.190	0.210	0.250
160	0.102	0.131	0.155	0.184	0.203	0.243
180	0.096	0.123	0.146	0.173	0.192	0.229
200	0.091	0.117	0.139	0.164	0.182	0.217

^an = The number of observations.

ACKNOWLEDGEMENTS

The author wishes to express his appreciation to Dr. R. S. Houk and Mr. R. J. Conzemius for their direction and assistance in the conduction of the research. I also wish to express gratitude to Drs H. J. Svec, H. A. David and R. E. McCarley as well as Mr. B. Beaudry for their help in bringing this work to completion. .

Our group is very much "instrument-oriented"; the TOF-MS studies could not have been done without skill, help, and assistance from machine shops and instrumentation services in Ames Laboratory. I would also like to thank my group members, S. Jiang and J. Crain for their aids and useful discussions, and we together (plus Sam Houk) occasionally work out some "international" jokes that make the "instrumental" group stimulating.

I am, finally, indebted to my wife, Feng Wang, and my parents for their patience and support throughout these "tough" years.